NPS-69PS-78-00

NAVAL POSTGRADUATE SCHOOL

Monterey, California

EFFECTS OF DISSIMILAR METAL COUPLING, POTENTIAL DISTRIBUTION, AND TEMPER CONDITION ON GALVANIC CORROSION OF 5086 ALUMINUM ALLOY IN SYNTHETIC SEAWATER

Jeff Perkins, J. S. Locke, and K. J. Graham

Materials Science and Chemistry Group
Naval Postgraduate School
Monterey, California 93940

January 1978

Technical Report No. 5
To the Office of Naval Research
Contract No. N00014-77-WR-70215
NR-036-120

NAVAL POSTGRADUATE SCHOOL
Monterey, California

Rear Admiral T. F. Dedman
Superintendent

Jack R. Borsting
Provost

The work reported herein was supported by the Office of Naval Research, Metallurgy Program Office, Code 471, Arlington, VA, 22217, through Contract No. N00014-77-WR-70215, NR-036-120.

This report was prepared by:

Jeff Perkins
Associate Professor of
Mechanical Engineering

LT John S. Locke, USN

K. J. Graham, Chemist

Reviewed by:

Paul J. Marto, Acting Chairman
Department of Mechanical Engineering

Released by:

William Tolles
Acting Dean of Research

UNCLASSIFIED
SECURITY CLASSIFICATION OF THIS PAGE (When Data Entered)

REPORT DOCUMENTATION PAGE	READ INSTRUCTIONS BEFORE COMPLETING FORM
(14) NPS-69PS-78-001, NPS-TR-5 (9) Interim rept. Mar-Dec 7	
(6) Effects of Dissimilar Metal Coupling, Potential Distribution, and Temper Condition on Galvanic Corrosion of 5086 Aluminum Alloy in Synthetic Seawater,	Interim, 3/77 to 12/77 Technical Report No. 5
(10) Jeff Perkins, J. S. Locke and K. J. Graham	N00014-77-WR-70215, NR-036-120
Materials Science and Chemistry Group, Code 69Ps, Naval Postgraduate School, Monterey, CA 93940	Program Element: 61153N Project: RR022-08-01
Office of Naval Research, Metallurgy Program Office, Code 471, Arlington, VA 22217	(11) January 1978
(12) 57p.	Unclassified

16. DISTRIBUTION STATEMENT (of this Report)
Approved for public release; distribution unlimited.
Reproduction in whole or in part is permitted for any purpose of the United States Government.

17. DISTRIBUTION STATEMENT (of the abstract entered in Block 20, if different from Report)
(16) RR022-08

18. SUPPLEMENTARY NOTES
(17) RR022-08-01

19. KEY WORDS (Continue on reverse side if necessary and identify by block number)
galvanic corrosion, 5086 aluminum alloy

20. ABSTRACT (Continue on reverse side if necessary and identify by block number)
The galvanic corrosion behavior of 5086 aluminum alloy in three tempers (H116, H117, H32) when coupled with more noble metals (1040 steel, naval brass, and Ti-150A titanium) and immersed in aerated synthetic seawater, was studied. Galvanic current density measurements, potentiodynamic polarization determinations, and optical and electron microscopic observations were made. Galvanic corrosion of 5086 aluminum was found to be independent of temper and to decrease in the order (of coupled metals) Ti > naval brass > 1040 steel.

DD FORM 1 JAN 73 1473 EDITION OF 1 NOV 68 IS OBSOLETE S/N 0102-014-6601 |
UNCLASSIFIED
SECURITY CLASSIFICATION OF THIS PAGE (When Data Entered)

251450

Block 20

The effect of dissimilar metal coupling decreases with time due to the formation of corrosion product deposits on both anodic and cathodic surfaces. Coverage of the surface of the aluminum (anodic) member of couples with corrosion products tends to promote the operation of local corrosion modes. Correlations have been made between corrosion product distribution and the distribution of dissolution attack by microscopic means, and the relation of these features to potential distribution is discussed.

Effects of Dissimilar Metal Coupling, Potential Distribution, and Temper Condition on Galvanic Corrosion of 5086 Aluminum Alloy in Synthetic Seawater

Jeff Perkins, J.S. Locke, and K.J. Graham

ABSTRACT

The galvanic corrosion behavior of 5086 aluminum alloy in three tempers (H116, H117, H32) when coupled with more noble metals (1040 steel, naval brass, and Ti-15CA titanium) and immersed in aerated synthetic seawater, was studied. Galvanic current density measurements, potentiodynamic polarization determinations, and optical and electron microscopic observations were made. Galvanic corrosion of 5086 aluminum was found to be independent of temper and to decrease in the order (of coupled metals) Ti > naval brass > 1040 steel. The effect of dissimilar metal coupling decreases with time due to the formation of corrosion product deposits on both anodic and cathodic surfaces. Coverage of the surface of the aluminum (anodic) member of couples with corrosion products tends to promote the operation of local corrosion modes. Correlations have been made between corrosion product distribution and the distribution of dissolution attack by microscopic means, and the relation of these features to potential distribution is discussed.

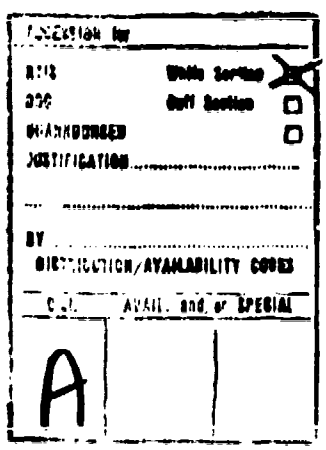

CONTENTS

1. Some Problems with 5000 Series Aluminum Alloys in Marine Applications

The use of aluminum for marine applications dates back to 1890 when the 5.2 m vessel "Zepher" was launched. By 1960 more than 1000 merchant ships were using substantial amounts of aluminum for structural applications. In contemporary U.S. Navy ships, most of the superstructure above the main deck is made of aluminum, and many other uses for aluminum are found throughout the ship. For example, the USS DEWEY (1959) was built containing about 167 tons of aluminum, mostly 5456-H321 plate and 5086-H32 sheet. Contemporary aircraft carriers such as the USS INDEPENDENCE (1958) carry about 900 tons of aluminum while a GEORGE WASHINGTON class submarine (1959) has about 20 tons of aluminum. Additionally many all-aluminum craft, such as submersibles and patrol boats, have been and are still being built. Since the use of aluminum saves weight, we can expect use in ever-increasing quantities, especially in forthcoming generations of high speed surface effect ships and craft.

Aluminum has good corrosion resistance to the atmosphere and to many aqueous media. It is a reactive metal, being very active in the EMF series, but develops an oxide surface film that protects it in many environments; this behavior can be inferred from examination of the Pourbaix (potential-pH) diagrams for aluminum. Thus the corrosion behavior of aluminum is determined essentially by the formation and behavior of a passivating layer of oxide film. The structure of the oxide film is generally complex. It may consist of Al_2O_3 alumina, $Al_2O_3.H_2O$ bohmite, $Al_2O_3.2H_2O$ bayerite or $Al_2O_3.3H_2O$ hydragillite (1). Hart (2) showed that the film formed on pure aluminum immersed in water (at temperatures less than 60°C) develops in three stages: first amorphous hydroxide is formed, then orthorhombic γ-AlO·OH and then bayerite. The final film according to Hart is then made up of three layers. The film of "Al_2O_3" is estimated to be 20°A to 100°A thick when formed in air.

Aluminum alloys with Mg content up to three percent have corrosion resistance about the same as pure aluminum and low mechanical strength (3). Increasing the amount of Mg increases the strength of the alloy but lowers its corrosion resistance somewhat. This is due to the magnesium being more anodic than the aluminum. The aluminum alloys designated 5086, 5456 and 5083, containing four to five percent magnesium, are used extensively in marine vehicle applications. In addition to corrosion resistance, they have good weldability and high strength to weight ratio (3). Typically, the strain hardened tempers designated as 5086-H32, 5083-H321 and 5456-H321 were selected.

It is well-known by naval architects and marine engineers that galvanic corrosion tends to occur when (5XXX series) aluminum alloys are coupled with other structural metals, which are typically more noble than aluminum. Therefore, features for prevention

of this type of corrosion are typically incorporated into the designs of marine vehicles using aluminum, for example, through the use of insulating materials to prevent electrical contact and paint coastings to prevent electrolyte contact with a dissimilar metal. However, for a variety of reasons galvanic corrosion problems still occur (4,5). For example, Strasburg (4) reported on the considerable expenditure of maintenance effort required to repair damage at the aluminum superstructure to steel deck interface on destroyer type ships, and also noted that there may be extensive corrosion damage on aluminum plate adjacent to pipe penetrations. Corrosion problems were also encountered in the bilge areas of aluminum-hulled (5456-H321) patrol boats used in Vietnam (5). These boats experienced extensive exfoliation corrosion. The conditions that existed in the bilge areas of the boats were extremely favorable to the initiation of pitting corrosion. Pitting would start and then give way to exfoliation or intergranular corrosion once the interior metallurgical structure of the alloy was exposed.

Exfoliation susceptibility of 5456-H321 is considered to be related to an elongated grain structure with relatively continuous precipitation of Al_3Mg_2 phase along the grain boundaries (5). The H32 and H321 tempers apply to products which are strain hardened and then stabilized by a low-temperature heat treatment to slightly lower the strength and to increase ductility and stress-corrosion resistance, a process which results in a microstructure in which the precipitate is present in a continuous line. Doig and Edington (6), in their work with a Al-7.2 percent Mg alloy, explained that the microstructure may be divided into three regions: the grain boundary precipitate of Al_3Mg_2, its associated solute depleted zone, and the matrix with bulk composition. The corrosion response is determined by the respective electrochemical properties of these three regions. The Al_3Mg_2 phase is more anodic than the matrix or the adjacent solute-depleted zone (6), so that this precipitate is preferentially attacked, and the corrosion products which form occupy more space than the metallic compound, and therefore exert a force on the metal. This causes delamination, the phenomenon called "exfoliation".

To prevent exfoliation, the continuous network of the Al-Mg precipitate must be broken up. To do this Reynolds and Alcoa recently developed the H116 temper and H117 temper respectively, for both 5456 and 5086 alloys. The H116 and H117 tempers apply to products which are strain hardened less than quarter-hard and do not undergo a stabilizing heat treatment. These alloys both have a grain structure predominately free of continuous grain boundary network, as opposed to the continuous grain boundary network found in the H32 and H321 tempers. Even with these tempers, continuous precipitate (sensitization) can be induced by natural aging. Since 5456 contains five percent Mg while 5086 contains only four percent Mg, this problem occurs more

readily in 5456 (7), and work by Czyryca and Hack (8) suggests that the H116 temper produces material less susceptible to natural aying. In general, the use of the H116 and H117 tempers should give improved performance with respect to exfoliation and intergranular corrosion. However, corrosion will still occur whenever galvanic couples are allowed to exist.

Even with the metallurgical advances mentioned above, and with other advances in corrosion control, galvanically induced corrosion between Al alloys and other metals is still a widespread problem in marine applications. In many cases the most efficient design requires the use of dissimilar metals, since criteria such as strength, fabricability, cost, availability and appearance are often weighed more heavily than corrosion control in the design process (9). Numerous examples can be cited. such as pipe penetrations through aluminum bulkheads, which usually brings steel and aluminum together. Watertight doors which penetrate the aluminum superstructure also provide a place for galvanic corrosion to take place. For strength reasons, brackets on aluminum bulkheads usually involve steel nuts and bolts. Heavy equipment mounted above the main deck usually requires steel for support and provides another opportunity for galvanic corrosion. To combat the severe corrosion that was occurring at the aluminum superstructure-steel deck interface, the U.S. Navy is now using an explosively bonded joint for repair of old corroded joints and for installation on new construction. The use of explosive bonded material eliminates the mechanical crevice normally present at the joint. However, when exposed to a corrosive marine environment, corrosion does occur preferentially at the bond interface as was shown by Keelean (10). The extent to which this detracts from the mechanical properties of the bond is unknown, but may be expected to be significant.

2. Galvanic Corrosion

Galvanic corrosion occurs when two or more metals in electrical contact are also in contact through an electrolyte. To predict the behavior of a metal in a galvanic couple, galvanic series are often used. Such series are constructed by listing the different metals according to their equilibrium potentials in a specific environment. For example, a galvanic series of some metals in flowing sea water is given by LaQue (11). The metal with the more active potential becomes the anode, while the metal with the more noble potential becomes the cathode when two dissimilar metals are coupled. The damage incurred by coupling the two metals is dependent on many factors, one of which is separation on the galvanic series (open circuit potentia difference). However, it is not possible to simply assume that the further apart (greater the potential difference), the greater the damage; it is essential to also consider the area ratio of the two metals in the particular situation, the polarizatio behavior of the metals, and the conductivity of the electrolyte. The simple approach

selecting metals based on position in a galvanic series can be a very poor indicator of galvanic corrosion rates, as pointed out recently by Mansfeld and Kenkel (12).

When two metals in a electrolyte are coupled, both metals are polarized so that each corrodes at a new rate; the more active metal corrodes more and the more noble metal corrodes less. The polarization is defined as the extent to which the potential of a metal is changed due to the induced galvanic current. The more active metal is polarized along its anodic polarization curve in the direction of increasing potential (becoming more noble in potential); the more noble metal is polarized along its cathodic polarization curve in the direction of decreasing potential (becoming more active in potential). Thus the respective behavior of the metals as they are polarized is extremely important in determining the final equilibrium potential between the two metals, the galvanic corrosion current, and the ensuing metal dissolution of the anode.

3. Methods to Study Galvanic Corrosion

Techniques for predicting galvanic corrosion include electrode potential determinations, current measurements, and polarization techniques. As pointed out by Baboian (13), only by using all these methods can an overall characterization of the behavior of the metals in a galvanic couple be completed.

a. Potential Measurements

Potential measurements are generally used to construct a galvanic series, which can be quite useful when the polarization characteristics for the metals are straightforward (14). However, there are other factors which can significantly decrease the usefulness of this method. For example, if a surface film forms so that the metal remains passive, then that film will influence the corrosion rate over a wide range of potentials. Also, the potential of a metal may vary with time, thus changing its position on the galvanic series. Additionally, the polarizability of the metal could change according to the environment and time. Thus the simple measurement of the corrosion potential, while useful, does not yield enough information on which to base a prediction of galvanic corrosion behavior.

b. Current Measurements

There are various ways to measure the current flowing between two electrically coupled dissimilar metals which are immersed in an electrolyte. The first and most obvious way is to measure the voltage drop across a known resistance. This method is generally considered unsatisfactory because the two metals are not at the same potential but are separated by the resistor voltage drop. This causes the measured current to be less than the actual galvanic current. Additionally, the reduced polarization associated with this situation may induce misleading conclusions when comparing results obtained for various dissimilar metal couples which have

different polarization characteristics. Early attempts to remove the effect of the resistor were described by Brown and Mears in 1938 and referenced recently by Mansfeld and Kenkel (12); basically, the resistor effect can be accommodated by using a set of switches and balancing circuitry. However, this introduces transients when the system is not in balance, which requires a recovery period, and cannot be used for continuous observations. Numerous investigators have had success using clip-on-milliammeters to measure the current through low resistance wire connecting the coupled metals. However, this method is typically limited to currents greater than 300 μA. The systems currently in greatest use take advantage of operational amplifiers to maintain a zero potential difference between the two dissimilar metals while measuring by some means the current required to do this. The balancing current then equals the galvanic current. An "electronic zero resistance ammeter with instantaneous null characteristics" was developed by Henry and Wilde; the principle of operation is based on the use of an operational amplifier to replace manual balancing, with the galvanic current read on a microammeter. It is also possible to use a potentiostat as a zero resistance ammeter (12), in which case, with the potentiostat set at zero millivolts applied potential, the galvanic current can be read directly on the current meter of the potentiostat.

c. Polarization Measurements

Polarization behavior is critically important relative to corrosion rates, since single metals that corrode uniformly may undergo severe localized corrosion when polarized, or may become passive. Therefore it is important to know the shape of the respective potential versus current curves in order to be able to predict the equilibrium potential and current density of coupled metals. This may be done by adding the currents of the cathodic curves to get a total cathodic curve and the currents of the anodic curves to get a total anodic curve. The intersection of the total anodic and total cathodic curves gives the equilibrium potential and current density of the couple. Or, if the potential of the couple has already been measured, then the current density may be predicted by finding the interaction of the horizontal line equal to the potential and the Tafel slope of one of the particular metals.

4. Objectives of this Research

The specific objective of the present research was to investigate and characterize the behavior of aluminum alloy 5086 when coupled with other, more noble, metals and immersed in seawater. In so doing, it was intended to add to the understanding of the basic mechanisms involved in galvanic corrosion situations. 5086 aluminum was selected because of its widespread use in marine applications. Also, it was of interest to compare the behavior of various tempers of this alloy, including the recently developed new tempers intended to reduce exfoliation susceptibility.

The general plan of attack was to corrode bimetallic couples in synthetic seawater for various lengths of time while monitoring the electrochemical behavior, after which the corrosion product formation and distribution would be studied macroscopically and microscopically. Polarization curves and galvanic current density data would be used to gain an understanding of the dynamics associated with the different couples and to correlate macroscopic and microscopic data with the electrochemical processes that had taken place.

Three metals noble in potential to aluminum were selected as the cathodic counter electrode, based on their open-circuit potential positions in the galvanic series for flowing seawater. The three were selected so that one (steel) was near aluminum in potential, one (titanium) was near the noble end of the galvanic series and the third (brass) was roughly half-way in between.

EXPERIMENTAL PROCEDURES

1. Materials

Aluminum alloy 5086 was obtained in H32, H116, H117 tempers. The 5086-H32 alloy was in the form of 0.483 cm thick sheet, manufactured by Alcan Aluminum Corp. The 5086 H116 alloy was in the form of 0.483 cm thick sheet, manufactured by Kaiser Aluminum. The 5086-H117 alloy was obtained on request from Mare Island Naval Shipyard, Vallejo, CA, in the form of 1.427 cm thick plate, not marked as to the manufacturer. 5086 aluminum alloy has a specified nominal percentage chemical composition of 0.45 Mn, 4.0 Mg, 0.15 Cr, balance aluminum, with compositional limits of 0.2 to 0.7 Mn, 3.5 - 4.5 magnesium, 0.05 - 0.25 Cr, 0.5 iron, 0.4 silicon, 0.25 zinc, 0.1 copper, and 0.15 titanium.

The microstructures of the 5086 Al alloy in the respective as-received tempers are shown in Figure 1. These structures are in agreement with those published by other researchers [6,9,11,12]. The 5086-H116 microstructure consists of a discontinuous network of precipitate, while the 5086-H32 has a more continuous network. The microstructure of the 5086-H117 seems to contain a somewhat more continuous precipitate network than 5086-H116, for the same metallographic preparation, which is not normally expected and may be caused by prior sensitization. It has been reported that there is a greater tendency for material in the H117 temper to become sensitized (than material in the H116 temper) (8). In any case, these microstructural variations will later prove to have little effect on the response of the aluminum alloy studied in these present experimental conditions. The cathodic metals used were 1040 steel, naval brass, and Ti-150A titanium.

2. Exposure of Proximate Couples

The primary purpose of these exposures was to deploy various proximate, planar, bimetallic couples in synthetic seawater in order to subsequently study corrosion product morphology and distribution. The anodic member of the proximate couples was in all cases one of the three temper types of 5086 Al, while the cathodic member was one of the three other metals (steel, brass, or titanium). Testing was accomplished by mechanically mating the two metals in such a way that a reproducible and crevice-free interface was produced. The samples were so designed that they could subsequently be examined in a scanning electron microscope (SEM) without disturbing their corrosion product formations. In the design of all test procedures, the guidelines set down in National Association of Corrosion Engineers Standard TM-01-69 were carefully followed (15). The exposure apparatus consisted of an array of 1000 ml beakers (Figure 2) each filled with 1000 ml of synthetic seawater prepared according to Kester et al (16).

this was accomplished by pumping air from an aquarium type pump through a system of rubber hose into each beaker via a small glass tube. Volume control of the air was accomplished by adjusting screw type clamps located on each hose, with the pump hose, vented to the atmosphere, used to reduce back pressure. The beakers were covered with watch glasses to prevent contamination and reduce evaporation.

Hydrogen ion concentration was monitored with a Photovolt Corporation Model 115 Electronic pH meter. A Beckman pH.9.18 buffer was used to standarize the instrument prior to use. pH measurements averaged 8.22 and varied from 8.1 to 8.5. Conductivity was monitored with a Barnstead Conductivity Bridge Model PM-70CM and a sensing electrode set as shown in Figure 6. The bridge and electrode set combination were calibrated using a 0.020 normal KCl solution. A correction factor of $404.cm^{-1}$ was computed. This factor was divided by the bridge reading in ohms to get conductivity in millimhos per cm. Conductivity measurements averaged 48.6 millimhos per cm and varied from 47.0 millimhos per cm to 49.9 millimhos per cm. The temperature of the corrosive medium was allowed to fluctuate with room temperature, which averaged about 21.5°C and varied from 18°C to 24°C, with average day/night variations of about $\pm$ 1.5°C.

A Cambridge Model S4-10 Stereoscan Scanning Electron Microscope (SEM) was utilized to study the corrosion product morphology and distribution and the damage resulting from the corrosive attack, together with a Princeton Gamma Tech PGT-1000 energy-dispersive x-ray spectrometer, and various light microscopes and macrophotographic equipment.

Nine couple types were studied as follows:

	ANODE	CATHODE
1.	5086-H32 Al	1040 Steel
2.	5086-H32 Al	Naval Brass
3.	5086-H32 Al	Ti-150A Titanium
4.	5086-H116 Al	1040 Steel
5.	5086-H116 Al	Naval Brass
6.	5086-H116 Al	Ti-150A Titanium
7.	5086-H117 Al	1040 Steel
8.	5086-H117 Al	Naval Brass
9.	5086-H117 Al	Ti-150A Titanium

The six different metals involved were milled into test coupons 1 cm by 1 cm by 0.48 cm. In the case of the Al, at least one face was left in the as-received condition so that it could later be mounted exposed to the synthetic seawater with

the direction of rolling horizontally oriented. Individual coupons were first mounted in a cylindrical plastic mount, in thermosetting resin, with one of the 1 cm by 0.48 cm sides exposed. The exposed side was lightly sanded flat on a 180 grit belt sander. The coupon was then broken out of the plastic sanding mount, and a bimetallic couple with a flat, tight, electrically conductive joint formed by joining the sanded surfaces of pairs of dissimilar metals. A special mounting ring device was used to form the bimetallic couple, as shown in Figure 2b. This consisted of a metal moulding ring into which were drilled and tapped two diametrically opposed holes; through these holes were threaded two 4-40 thread screws which were tightened, using a mini-torque wrench, to 0.7N·cm, therefore pressing the metals together with a constant and reproducible stress. Thermosetting resin was then poured into the ring and allowed to harden. After the resin had set, the screws were removed and the mounted couple removed; the finished couple is shown to the right in Figure 2b. The sample was then sanded with a 50 grit belt sander on both the front and back to remove excess plastic. This was done on the front only to the point that metal was exposed. On the back however a large portion of the plastic was removed to thin the sample so that it would more conveniently fit on the SEM stage; the sample back was ground so as to expose the back of the couple, and allow direct contact to the SEM stage. Grinding was completed by sanding the face of the sample to an 000 grit finish. The samples were then cleaned ultrasonically in tap water, rinsed in alcohol and blow dried with warm air. The exposed backs of the samples and the holes left by the bolts were filled with paraffin prior to exposure. The above procedure was able to produce a high quality, crevice-free, planar cathode: anode joint as shown in Figure 3a.

Different samples were immersed for one day, one week, two weeks, three weeks, and eight weeks. After the specified exposure period the individual sample was removed from the synthetic seawater and dipped in distilled water for about three seconds. After dipping, photographs were taken of the condition of the sample while still wet and also after drying, using both a low power light microscope and a 35mm macro camera. The sample was then examined in the SEM, using the energy dispersive X-ray spectrometer when required. After initial SEM observations, the samples were ultrasonically cleaned of corrosion products using distilled water and a commercial cleaning product called "Micro" mixed to the manufactures recommendations. After cleaning, they were rinsed in distilled water, rinsed in alcohol, and air dried. Observations of corrosion damage were then made using the SEM.

3. Galvanic Current Density Measurements

The purpose of these measurements was to determine, for separated bimetallic couples which were as similar as possible geometrically to the proximate couples,

the galvanic current between the dissimilar metals. These measurements would give an indication of the corrosion rates of the various couples, which could then be correlated with surface observations made on the proximate couples and with potentiodynamic polarization measurements.

The corrosion cells used for these measurements consisted of beakers filled with 1000 ml of synthetic seawater. Oxygen concentration was maintained at a constant saturated level through the use of an air sparging system arranged as previously shown for the physically coupled cells, and the beakers covered with watch glasses. A Princeton Applied Research Model 173 Potentiostat/Galvanostat was used as a zero impedance ammeter, and galvanic current was measured as a function of time for all nine couple types. The samples for these measurements consisted of separately mounted anode and cathode test coupons, otherwise prepared exactly as for the proximate couples, with provision made for electrical contact to and between the dissimilar metals by threading copper wire into the side of the mounted coupons and sealing with paraffin.

4. Potentiodynamic Polarization Measurements

The purpose of these measurements was to obtain the characteristic anodic and cathodic polarization curves for the various metals being tested. This data would be useful in making interpretations of the galvanic current density data and the observations of corrosive attack on the coupled samples. A Princeton Applied Research Model 173 Potentiostat/Galvanostat was used, with a standard polarization cell and calumel reference electrode. The auxiliary electrodes were graphite rods. Preparation of the polarization test coupons was identical to that used for the measurement of galvanic current.

RESULTS AND DISCUSSION

1. Potentiodynamic Polarization Behavior

Potentiodynamic polarization curves for the six test metals are shown in Figures 4-6. The anodic polarization curves were essentially identical forall three tempers of the 5086 Al alloy, indicating that the tendency of this Al alloy to corrode in a galvanic couple may not be dependent, at least macroscopically, on its temper condition. Also shown in Figures 4-6 are the respective cathodic polarization curves for the three more noble metals deployed in the galvanic couples. The intersection points obtained allow an approximation of the galvanic current density which would be experienced for a given couple, i_{couple}, and the corrosion rate for the anodic metals can also be predicted. The predicted galvanic current density, i_{couple}, for the three types of couples, taken from Figures 4-6, are: 112 $\mu A/cm^2$ for the brass/Al couple, 60 $\mu A/cm^2$ for the steel/Al couple, and 37 $\mu A/cm^2$ for the Ti/Al couple. This ordering of i_{couple} (brass/Al > steel/Al > Ti/Al) would not be obvious from the relative position of these materials in galvanic series for seawater, where the potentials of the three cathodic materials are ordered Ti > brass > steel. The observation that galvanic series open-circuit potential differences cannot be taken as an indicator of dissolution rates has recently been demonstrated by the extensive work of Mansfeld and Kenkel (17), who recommend that galvanic series be considered as only "very qualitative guidelines".

Also from the single metal polarization curves, the equilibrium potentials, E_{corr}, of the independent metals is determined, and E_{couple} for each couple type can be predicted. The E_{corr} values were measured (all vs. SCE) as: -0.22 V for Naval Brass, -0.36 V for Ti-150A, -0.52 V for 1040 Steel, and -0.76 V for 5086 Al, while the values for E_{couple} were predicted to be (all vs. SCE): -.725 V for Ti/Al, -.715 V for brass/Al, and -.720 V for steel/Al. According to the galvanic series in flowing seawater developed by LaQue, the potentials of these materials are in the order: Ti > brass > steel > Al. The measurements made in this work show a reversal in the positions of the brass and Ti potentials. Again a difficulty in gaining sight from conventional galvanic series presentations is exemplified. Mansfeld and Kenkel (17,18), for conditions similar to the present experiments, recently reported corrosion potential results very close to those recorded here, for similar alloys immersed in aerated 3.5 percent NaCl. A comparison of the measured potentials is shown in Table I.

TABLE I

Comparison of Equilibrium Potentials
(vs. SCE) for Various Metals

Present Work (synthetic seawater)		Mansfeld and Kenkel (17,18) (3.5 percent NaCl)	
Material	E_{corr}	Material	E_{corr}
Naval Brass	- 0.22V	Cu	- 0.237V
Ti-150A	- 0.36V	Ti-6Al-4V	- 0.352V
1040 Steel	- 0.52V	4130 Steel	- 0.591V
5086 Al	- 0.76V	6061-T651 Al	- 0.756V

The curves of Figures 4-6 illustrate the importance of the polarization behavior of the respective metals in the couples, especially the cathodic polarization behavior. For example, steel has a lower E_{corr} value than either brass or titanium, yet the predicted value of i_{couple} for steel/Al couples is midway between the values predicted for Ti/Al and brass/Al couples. This can be related to the polarization behavior of the respective cathodic metals. Ti polarizes to a greater extent than steel (i.e., the current density for Ti does not increase as fast with decreasing potential), and intersects the Al anodic polarization curve at a lower value of current density. Brass, with the highest single metal value of E_{corr}, also obtains an i_{couple} intersection which is the highest of the three couple types examined here. The relatively low galvanic current obtained for the Ti/Al couple is due to the character of the titanium cathodic polarization behavior, which has been noted by other workers (19,20).

The results of any potentiodynamic polarization experiment are exactly applicable only for the test conditions (in this case, 1 mv/sec scan rate, etc.). Thus the results of these short-immersion-time polarization tests can only serve as an approximation to the long-term corrosion behavior. It was for this reason that galvanic current vs. time data was also collected.

2. Galvanic Current Density

First, it is of interest to check the degree of correlation between galvanic current density versus time data and the potentiodynamic polarization measurements. The galvanic current densities which would be predicted on the basis of the polarization curves would be ordered as lowest for Ti/Al, higher for steel/Al and highest for brass/Al. This ordering is realized, but only for the initial (t=0) i_{couple}

values recorded when monitoring i_{couple} vs. time for actual couples, as presented in Figures 7-9. Each of the Figures 7-9 show three curves, representing the results of three separate tests in which the temper of the Al alloy was common. For example, the three curves in Figure 7 represent galvanic current density versus time for 5086-H32 coupled to the three different cathodic metals.

The curves shown in these figures have certain characteristics in common. For couples in which the Ti is the cathodic metal, i_{couple} starts low (about 45μA/cm^2), rapidly increases to a plateau (about 75μA/cm^2), then gradually decreases to about 33μA/cm^2. As mentioned, the initial i_{couple} value is very close to that determined from the intersection of the Al and Ti polarization curves. The subsequent increase in current with time from this initial value is considered to be caused by the build up of an oxide film on the initially "clean" Ti surface. Since titanium is a reactive metal, it normally depends on a protective film of TiO_2 for corrosion resistance. The sanding involved in the sample preparation procedure in these experiments removed the oxide layer, thus making the metal potential more active (closer to that of Al). The initial rise of current is believed to be associated with passivation of the Ti surface by oxide layer growth after immersion. This causes the potential to become more noble, and a greater potential difference with the aluminum is obtained. Such behavior has been noted by Pettibone and Kane (20) who report that the potential of Ti changes from -0.8V when first immersed to -0.1V "after a matter of minutes" due to the development of a protective oxide coating.

The sharp initial rise in current density shown by couples involving Ti was in contrast to the behavior of couples with brass or steel. The galvanic current for brass-coupled aluminum samples typically started relatively high (about 100μA/cm^2) (again, as predicted by the polarization curves), decreased rapidly to about 70μA/cm^2, and then showed a gradual decrease to about 30μA/cm^2 after twenty-four hours. Couples with steel did not start as high (about 60μA/cm^2) and after an initial decrease dropped gradually to about 30μA/cm^2 after twenty-four hours. The initial drop in current exhibited by couples with steel or brass can probably be attributed to the initial formation of corrosion product on the Al anode.

Once past the initial transient period (of approximately one hour duration) the current density vs. time curves for various couples maintain the same relative position with the current densities being ordered from high to low as: Ti/Al, brass/Al, steel/Al. It is interesting to note that this ordering is consistent with that which would be predicted using the traditional criteria of position on the galvanic series.

To calculate the average values of galvanic current density for each curve a simple numerical integration scheme was used, by computing the area under each curve and dividing by the total time. The calculated average i_{couple} values are shown in Table II.

TABLE II

Average Galvanic Current Density ($\mu A/cm^2$)

	Temper of Al Anode		
Cathode	H32	H116	H117
Ti-150A	60	60	57
60/40 Naval Brass	51	50	52
1040 Steel	37	40	38

The data in Table II is quite consistent, with the average galvanic current density being higher for more noble cathodic metals. Once again, the observation is that the corrosion rate of the coupled Al alloy can be ordered from high to low as: Ti/Al, brass/Al, steel/Al. In these experiments, the galvanic corrosion rate of the 5086 aluminum alloy was not observed to be affect by temper condition. It was observed that at the end of the twenty-four hour test period the current density for all couples are converging to a level of about $30\mu A/cm^2$. The gradual decrease toward this value is probably caused by a stabilization of the corrosion product accumulation process on the Al anode. In terms of the polarization curves, one can speculate that the slope of the anodic Al corrosion curve is increasing, and is the major determinant of the observed decay of i_{couple} with time. These ideas regarding anodic corrosion product formation were explored further through macroscopic and microscopic examination of coupled samples, some of which were immersed for much longer periods.

3. Morphology and Distribution of Corrosion Products on Proximate Galvanic Couples

a. Morphology and Distribution of Precipitate Formations on Cathodic Members of Couples

Macroscopically, most of the cathodic members of the coupled samples appeared to have little precipitate formation on their surfaces. Figure 10 is a macrophotograph taken with a polaroid camera attached to a low power light microscope and is typical of the photographic records made of the physically coupled samples after drying. These photographs and the SEM photographs included in this work are all oriented on the pages in the same way that they were hung in the water; the top of the photo represent the top of the samples as they were exposed; in photographs presenting a vertical couple interface, the Al is on the right side in the photo. Figure 10 represents a couple exposed for two weeks; the cathodic member shows only small amounts of precipitate deposit. Another typical sample is shown in Figure 11 for a two day exposure. There is an accumulation of precipitate on the cathode that seems to be streaming from the vicinity of the anode/cathode joint, as seen more clearly in Figure 11b, a higher magnification SEM view of the interface area. The observed directionality evident in the precipitate distribution is due to the gentle circulation pattern in the beaker, and indicates that the precipitate is corrosion product from the Al anode which has been deposited on the cathode.

Higher magnification examination of the cathodic accumulation of precipitate on many samples showed that there are some general characteristics of deposit morphology on the cathodic areas, as illustrated in Figure 12. An extended, ridge-like formation was the general morphology observed (Figure 12), along with a more complete base layer covering the cathodic surface (Figure 13). Details of the base layer, which was present on all cathodic samples, were observable at higher magnification, where it is seen to consist of an array of very fine crystallites (Figure 13). Analysis (by energy-dispersive X-ray spectroscopy) of the cathode-located ridge-like formations and the base layers showed that these are both aluminum-based compounds. Therefore it is obvious that these cathode-located products have their origin in anodic dissolution processes. The mechanism by which they form and are transported to the cathodic surfaces is not completely clear at this time. Also, because of the small size of the samples used in this work, there was no indication of the distance over which this coverage might extend. The observation of aluminum-based compounds

on coupled cathodic surfaces was earlier reported by Keelean and Perkins (9) in work on the marine corrosion of aluminum: steel explosively bonded joints.

Another interesting structure observed on cathodic surfaces, which will be described as "corn husk" formations, is shown in Figure 14. Unlike the features mentioned earlier, these features were found on only a few of the samples; analysis of these features using the energy-dispersive X-ray analyzer (Figure 14cd) reveals that they are a calcium compound, devoid of Al. However, the surface of the metal upon which they stood is covered with an Al compound.

These observations confirm the existence of extensive product and precipitate formations on the cathodic members of galvanic couples after seawater exposures. These structures can insulate the cathode and thereby reduce the net galvanic effect. The effect on the anodic member would be to lower the galvanically induced corrosion rate, as indicated by the galvanic current density measurements presented earlier. Note that none of the observed structures represent artifacts, such as sea salts deposited after evaporation, as trials with the rinse and drying procedure have proved. In order to further investigate the effects of corrosion-related product structures, the corrosion products and associated damage to the Al alloy anodic members of couples were also studied.

b. Morphology and Distribution of Corrosion Products on Aluminum Alloy Anodic Members of Couples

Macroscopically, the morphology of the corrosion product on the Al anodic members of couples typically appeared as a white product with no distinct form, as seen in Figure 15; this is undoubtedly an accumulation consisting principally of various forms of hydrated Al_2O_3. Examination using SEM showed (at relatively low magnification) that the structure of the corrosion product formed on the Al varies from a somewhat unevenly distributed structure (as shown in Figures 16a and 16c) to a more compact structure (as shown in Figure 16e).

At higher magnification the product, whether non-uniform or compact, has a white "snow-like" structure (Figures 16b and 16d). Morphological differences between individual deposits are evident. For example, in Figure 17a the deposits appear to be light and resemble the appearance of dry cold snow while the deposits shown in Figure 17b exhibit a more "globule"-like appearance much like wet snow. These morpholgoical differences may arise due to slight differences in the drying process and is probably not related to any particular variable of the corrosion exposure. These SEM-level observations of Al corrosion product morphology are similar to those reported by previous researchers. Wright (21) observed similar "snow-like" morphologies for corrosion products on Al sacrificial anodes. Some other examples of corrosion product morphologies observed in this study are shown in Figure 18.

Also shown in these figures is a base layer which seems to almost completely cover the anodic Al. This structure can be seen in Figure 18b in the upper right. The structure is quite thin, since one can still observe the original sanding marks on the base metal, to which the film conforms. At high magnification, this base layer is seen to have the same structural morphology as the base layer found on the cathodic surfaces (e.g. Figure 13) Keelean and Perkins (9) observed the presence of a similar coating.

These observations of corrosion product formations and coatings of the Al anode, together with the observed coatings on the cathodic metals, help to explain the previously-presented variations in galvanic current density with time. From these combined results certain conclusions regarding the galvanic corrosion processes of these bimetallic couples in seawater can be deduced. As previously described, the plots of current density versus time indicate that as the immersion time increased the current density curves converged to a level of about $30\mu A/cm^2$, and it was postulated that this must be due to the formation of insulating layers on the electrode surfaces. It is now confirmed that layers form and cover both the anodic and cathodic surfaces, at least in proximate couples. As a result of these observations, the question arises whether, due to the extent of these coatings, the galvanic effect becomes small, so that local corrosion modes on the individual metals, such as crevice corrosion and pitting, may flourish. In order to study this further, the distribution of corrosion products and dissolution damage on the anodic surfaces, was carefully examined as a function of time.

Visual examination of all samples taken as a group produced some general observations on corrosion product distribution. Corrosion product accumulations on the Al member of the couple tended to be greater with longer exposure times, as expected. Also, for exposures up to one week, couples containing H32 generally showed greater corrosion product accumulation than couples containing H116 or H117; this difference was no longer obvious when the exposure was extended to two weeks or greater, and was the only observation of a temper effect noted in this study.

Figure 19 illustrates features which were present on many samples. Typically, the edges of the exposed planar area of the Al were covered by a heavier accumulation of corrosion product, in contrast to the relatively uniform distribution over the central surface area of the sample. The cathode:anode interface was sometimes but not always covered by a heavier distribution; an interfacial outcropping (e.g. Figure 19a) was observed on about twenty five percent of the samples exposed. Other samples showed no special accentuation of corrosion product coverage at the cathode: anode interface (e.g. Fig. 19b). These variations cannot be correlated with any particular variable, such as immersion time, cathodic metal or temper of the Al alloy

The interface regions of proximate couples showed a number of interesting features. Of particular interest was what could be called a "corridor" on the Al, immediately adjacent to the build up of corrosion products at the interface, as shown in Figure 20. This "corridor", seen in the top middle of Figure 20a shows much less corrosion product on the Al immediately adjacent to the interface. Figure 20b shows a higher magnification view of the area under discussion. Areas such as this were prevalent on almost all samples, and were always most pronounced adjacent to heavy accumulations of corrosion product.

In these experiments, the cathode:anode interface typically experienced less accumulation of corrosion products than at the plastic mount:aluminum interfaces. An attempt to quantify this observation was made. The (one) galvanic interface and (three) plastic:Al interfaces of each aluminum coupon were rated as to light, moderate, or heavy accumulations of corrosion product. These ratings were then weighted, added, and averaged. This was done several times. The results always showed that the accumulation for the galvanic joints was slightly less than a moderate build up and the average for the Al plastic edges was slightly less than half way between a moderate and a heavy build up.

The results seem at first to be contrary to expectations based on traditional treatment of interactions in galvanic couples. It might be expected that the quantity of corrosion product build up and dissolution damage would be concentrated particularly at the cathode:anode interface and decrease smoothly as some function of distance (potential) away from that interface. This does not occur, largely due to the small size of the proximate coupons and the high throwing power (ionic conductivity) in these galvanic cells, so that the potential distribution is spread out.

The observed feature of a degree of increased attack at the plastic:Al interfaces occurred because the specimen design employed could not avoid some finite elevation difference at these interfaces (see Fig. 3), so that some concentration of electrode current occurs at these locations. Some of the results reported in the next section, for samples cleaned of corrosion products, will support these explanations of sample mount edge effects. It should be noted that these edge effects were not so great as to confuse observations of general corrosion product form and distribution over the members of the galvanic couples.

c. Distribution of Dissolution Damage

After cleaning corrosion products from the samples, correlations between corrosive attack and distribution of corrosion product were obvious. If an area showed a large accumulation of corrosion product, then after cleaning, a cavity or other form of concentrated corrosive attack was always observed beneath that

position. An example of this is shown in Figure 21. The macrophotograph (Figure 21a) shows a large accumulation of corrosion product at the top along the cathode: anode interface and a relative lack of corrosion product along the lower portion of the interface. Figures 21b and c show the damage incurred in those two areas, respectively. The base metal under the location of extensive corrosion product accumulation was severely attacked, whereas the region where there was less product accumulation had been only lightly attacked. This correspondence between accumulation and damage was also evident at locations along plastic:Al interfaces, and on the central areas of the exposed faces of the anode samples.

As previously shown, localized dissolution tends to occur at cathode: anode interfaces, and correlations between the position of concentrated dissolution and heavy corrosion product accumulations were readily apparent. Additionally, observations showed that even though a flat, tight metal-to-metal joint was present prior to immersion, localized attack at the interface rapidly opened up a crevice-like cavity along the interface; examples (for 2-day exposure) are shown in Figure 22. Variation in the extent of development of this interfacial cavity are associated with the observed variation in corrosion product accumulations along the joint mentioned earlier. Figure 23 shows examples of interfacial dissolution distribution after somewhat longer exposures.

From all these observations, some ideas can be developed which describe the sequence of events involved in the attack of the galvanically coupled anodic Al. Upon immersion, the raised edges of the Al at the plastic: Al interfaces and the cathode: anode interface act as current concentrating sites, due to the non-uniform geometry and the galvanic potential respectively. This action, together with the likely presence, or development of, slight crevices at the interfaces provide sites at which localized corrosion can take place. Since the potentials of the coupled cathodic metals are more noble than the critical pitting potential of the Al, dissolution will tend to start at these areas (and also possibly at other areas where imperfections exist in the oxide). As the other areas of the Al become more passive (covered with a protective oxide film) the unfavorable area ratio accelerates corrosion in areas that have started to dissolve. As the cathode and anode of the bimetallic couples become covered with deposits, and the total galvanic current decreases, areas which are being attacked most aggressively tend to "rob" current from immediately adjoining areas,producing the low-corrosion "corridors" observed next to the locations of highest attack. In effect, these "corridor" regions are being cathodically-protected by the locally pronounced anodic action. As time goes on the localized attack dominates the corrosion process and large dissolution cavities are developed.

CONCLUSIONS

The following conclusions have been reached as a direct result of this research.

1. Galvanically induced corrosion of 5086 Al alloy is independent of temper condition for the time period studied (less than three weeks).
2. The rate of corrosive attack of the 5086 aluminum alloy anodic member of couples, based on current density measurements, can be ordered from highest to lowest as Ti/Al, brass/Al, steel/Al (for 24-hour exposure trials).
3. Formation of insulating corrosion products and structures on both cathodic and anodic members of couples acts to reduce the effect of dissimilar metal coupling. The primary source of these films is dissolution of the anodic Al, upon which the Al corrosion product accumulates, or from which it can migrate to the cathodic member and accumulate. These coverage effects cause a decrease in galvanic current density with increasing exposure time.
4. Non-uniform development of corrosion products on the Al anodic member of couples leads to concentration of corrosive attack at localized areas. This causes severe dissolution attack to take place, and a cathode/anode relationship is developed with immediately adjacent areas.
5. Heavy accumulations of corrosion product on Al anodic members of couples are associated with directly underlying large dissolution cavities.

REFERENCES

1. M. Pourbaix, Atlas of Electrochemical Equilibria in Aqueous Solutions, 2nd ed., p. 168-175, National Association of Corrosion Engineers, 1974.

2. R.K. Hart, "The Formation of Films on Aluminum Immersed in Water," Transactions of the Faraday Society, 53(1957) 1020-1027.

3. D.O. Sprowls, "High Strength Aluminum Alloys with Improved Resistance to Corrosion and Stress-Corrosion Cracking", paper presented at the Tri-Service Corrosion Conference, Philadelphia, Pennsylvania, 26-28 October 1976.

4. W. Strasburg, "Survey of Corrosion Problems of Destroyer Type Ships," NAVSEC travel report ser 78-6101C, 25 January 1971.

5. T.J. Summerson, "Aluminum Association Task Group Exfoliation and Stress Corrosion Testing of Aluminum Alloys for Boat Stock", paper presented at Tri-Service Corrosion of Military Equipment Conference, Dayton, Ohio, 29-31 October 1974.

6. P. Doig, and J.W. Edington, "The Influence of Solute Depleted Zones on the Stress - Corrosion Susceptibility of Aged Al - 7.2 Mass % Mg and Al - 4.4 Mass % Cu Alloys," Proc. Royal Soc. London, 339 (1974) 37-47.

7. C.L. Brooks, "Aluminum - Magnesium Alloys 5086 and 5456 - H116," Naval Engineers Journal 82 (August 1970) 29-32.

8. E.J. Czyryca and J.P. Hack, "Corrosion of Aluminum Alloys in Exfoliation - Resistant Tempers Exposed to Marine Environments for Two Years", paper presented at Tri-Service Corrosion of Military Equipment Conference, Dayton, Ohio, 29-31 October 1974.

9. G.S. Haynes and R. Baboian, "Reducing Galvanic Corrosion with Transition Metals," Materials Performance 16(1977) 36-39.

10. M.R. Keelean and A.J. Perkins, "Microscopic Investigation of Interface Corrosion of Steel - Aluminum Explosively Bonded Material Exposed to Periodic Sea Water Spray", M.S.M.E. Thesis, Naval Postgraduate School, Monterey, CA, 1976.

11. F.L. LaQue, Corrosion Handbook, p. 416, Wiley, 1948.

12. F. Mansfeld and J.V. Kenkel, "Laboratory Studies of Aluminum Alloys," Galvanic and Pitting Corrosion - Field and Laboratory Studies, ASTM STP 576, pp. 20-47

13. R. Baboian, "Investigation of Galvanically - Induced Localized Corrosion," Localized Corrosion - Cause of Metal Failure, ASTM STP 516, pp. 145-163, American Society for Testing and Materials, 1972.

14. R. Baboian, "Electrochemical Techniques for Predicting Galvanic Corrosion," Galvanic and Pitting Corrosion - Field and Laboratory Studies, ASTM STP 576, pp. 5-19, 1976.

15. National Association of Corrosion Engineers, NACE Standard TM-01-69, "Test Method: Laboratory Corrosion Testing of Metals for the Process Industries", 1969.

16. D.R. Kester, I.W. Duedall, D.N. Conners, and R.M. Pytokowicz, "Preparation of Artificial Seawater," Limnology and Oceanography, (12)(1967) 176-178.

17. F. Mansfeld and J.V. Kenkel, "Electrochemical Testing of Galvanic Corrosion", paper presented at Tri-Service Corrosion of Military Equipment Conference, Dayton, Ohio, 29-31 October 1974.

18. F. Manfeld and J.V. Kenkel, "Laboratory Studies of Galvanic Corrosion, I. Two-Metal Couples, Corrosion, 31 (1975) 298-302.

19. F.L. LaQue, Marine Corrosion, pp. 194-195, Wiley, 1975.

20. J.S. Pettibone and R.L. Kane, "Titanium". Corrosion Resistance of Metals and Alloys, 2nd ed., edited by LaQue, F.L. and Copson, H.R., pp. 647-648, Reinhold, 1963.

21. P.W. Wright, "A Scanning Electron Microscope Study of the Corrosion of Sacrificial Hull Anodes under Simulated Ship Service Conditions", M.S.M.E thesis, Naval Postgraduate School, Monterey, CA, 1976.

LIST OF FIGURES

Figure 14: Precipitate formations occasionally found on cathodic members of proximate couples, shown here for brass/5086-H32 couples in aerated synthetic seawater: (a) exposed two weeks, 230X, (b) exposed eight weeks, 110X, (c) same, 550X, (d) calcium x-ray distribution image of same area.

Figure 15: Low-magnification photograph of naval brass/5086-H32 proximate couple exposed for one week in aerated synthetic seawater, 7X.

Figure 16: Typical corrosion product accumulations on 5086-H116 aluminum in proximate couples exposed in aerated synthetic seawater (a) 5086-H116 coupled to Ti-150A, exposed three weeks, 23X, (b) same, 1150X, (c) 5086-H116, coupled to 1040 steel, exposed one week, 150X, (d) same, 1150X, (e) 5086-H116 coupled to Ti-150A, exposed two weeks, 55X.

Figure 17: Typical variations in corrosion product morphology found on 5086 aluminum exposed in proximate couples in aerated synthetic seawater:
(a) 570X
(b) 1100X.

Figure 18: Examples of various corrosion product morphologies observed on 5086 aluminum exposed in proximate couples in aerated synthetic seawater.
(a) 5086-H32, coupled with 1040 steel, exposed one week, 2200X,
(b) 5086-H116, coupled with 1040 steel, exposed three weeks, 1100X,
(c) 5086-H32, coupled with 1040 steel, exposed three weeks, 540X,
(d) 5086-H32, coupled to naval brass, exposed one week, 575X.

Figure 19: Photographs of (a) 1040 steel/5086-H32 and (b) naval brass/5086-H32 proximate couples after one week exposure in aerated synthetic seawater, to illustrate the discontinuous distribution of concentrated attack along the edges of the aluminum coupons.

Figure 20: Concentrated corrosion product accumulation at bimetallic interface of Ti-150A/5086-H32 proximate couple exposed 3 weeks in aerated synthetic seawater: (a) 22X, (b) 52X. Note the relatively low accumulation of corrosion products in a "corridor" on the aluminum adjacent to the interface.

Figure 21: Illustration of correlation of corrosion product distribution and dissolution pattern, for Ti-150A/5086-H32 proximate couple exposed two days in aerated synthetic seawater: (a) low magnification photograph of couple, showing distribution of corrosion products along bimetallic interface; (b) dissolution cavity found in the aluminum after ultrasonic cleaning, located under the heavy corrosion product outcropping seen in (a) at the top along the interface, 100X; (c) no dissolution cavity is found further down the same interface, 550X.

Figure 22: Appearance of bimetallic interfaces of proximate couples after two-day exposures in aerated synthetic seawater, then ultrasonically cleaned of corrosion products: (a) naval brass/5086-H32 couple, 550X; (b) Ti-150A/5086-H116 couple, 600X; (c) 1040 steel/5086-H32 couple, 1050X.

Figure 23: Appearance of bimetallic interfaces of proximate couples after exposure in aerated synthetic seawater, then ultrasonically cleaned of corrosion products: (a) Ti-150A/5086-H32 couple, exposed for 2 weeks, then cleaned, 22X; (b) naval brass/5086-H32 couple, exposed 8 weeks, then cleaned, 550X.

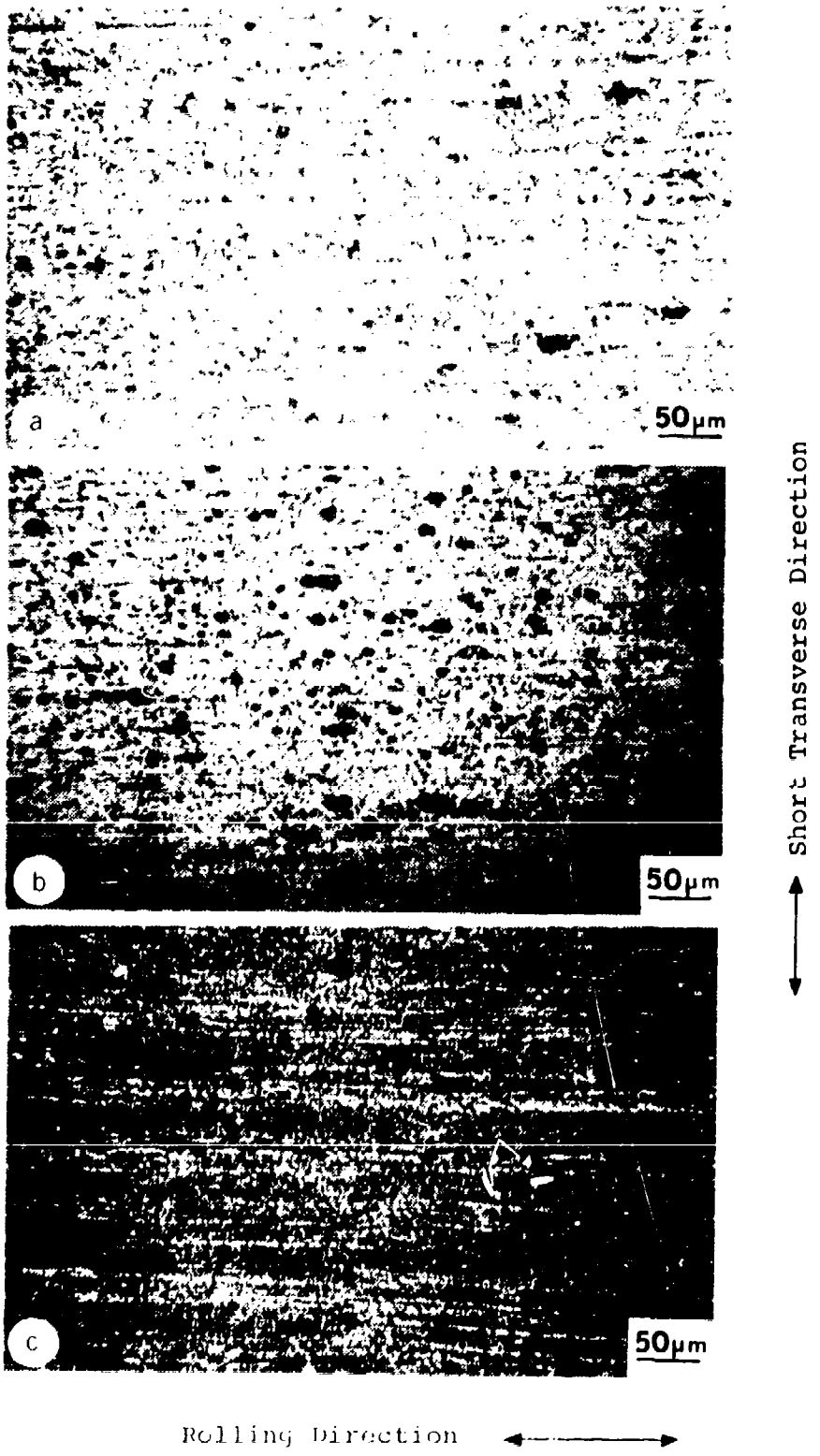

Figure 1: Microstructures of 5086 aluminum alloys used in these studies, all 200x, Kellers etch (a) 5086-H32, (b) 5086-H116, (c) 5086-H117.

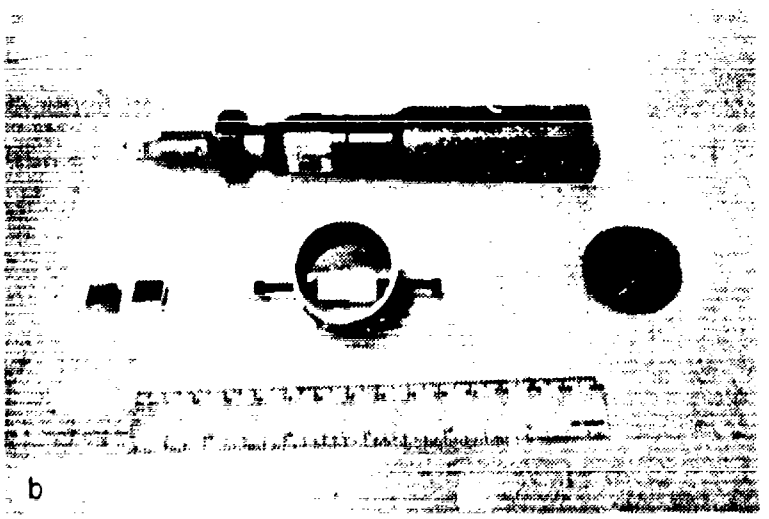

Figure 2: (a) Experimental equipment used for exposure of galvanic couples (b) Mounting equipment used to form proximate galvanic couples Shown are torque wrench, sample coupons, mounting ring, and final mounted couple.

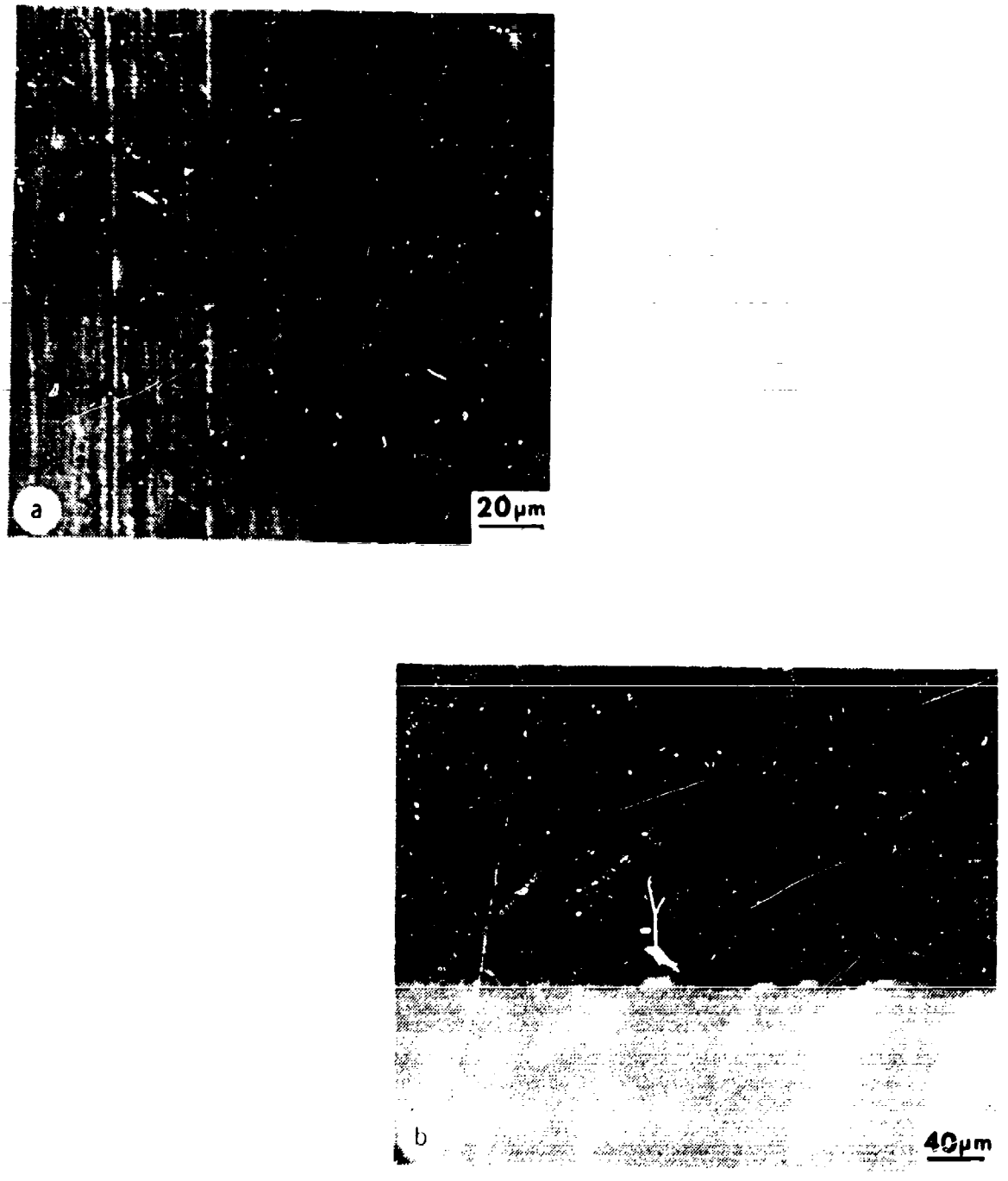

Figure 3: (a) Initial condition of bimetallic interface in proximate bimetallic couples, 550x. (b) Initial condition of metal: plastic interfaces of mounted samples, 240x.

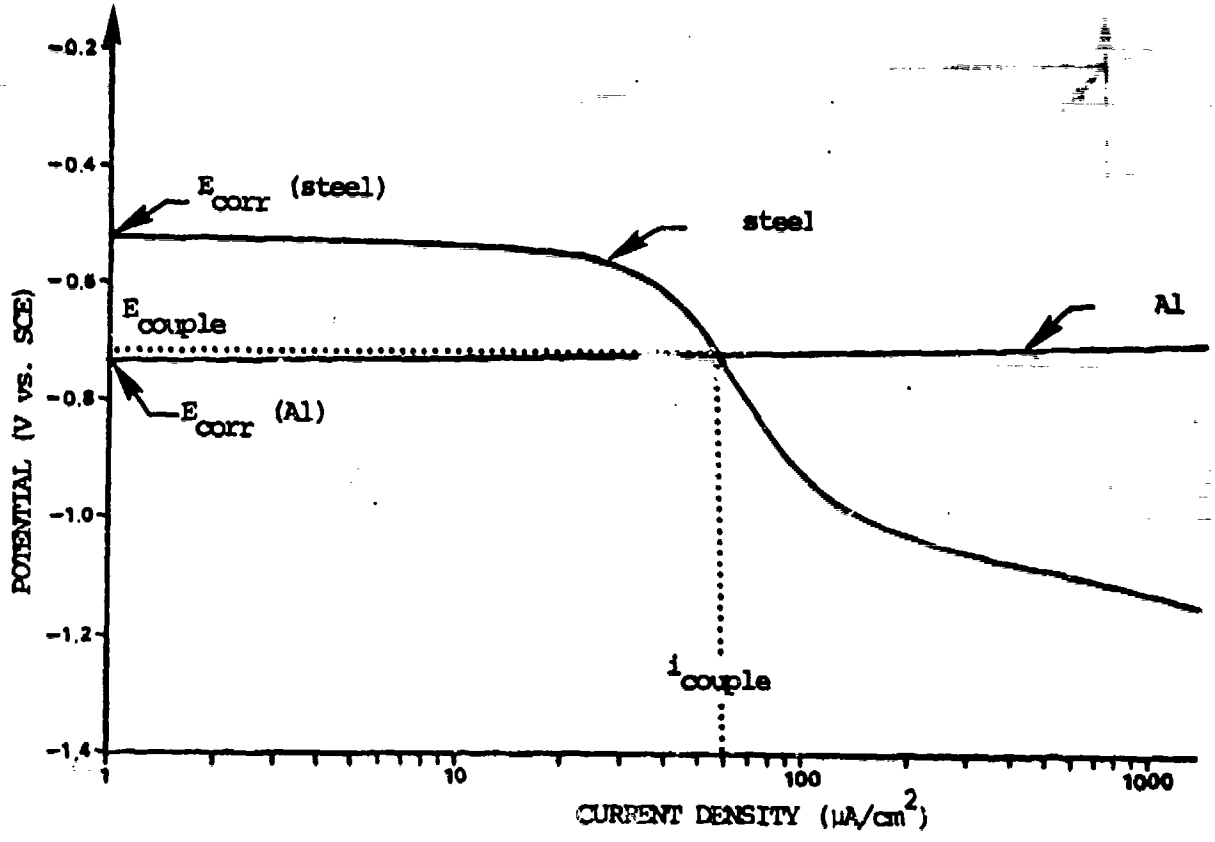

Figure 4: Potentiodynamic polarization curves for 5086 aluminum and 1040 steel in aerated synthetic seawater.

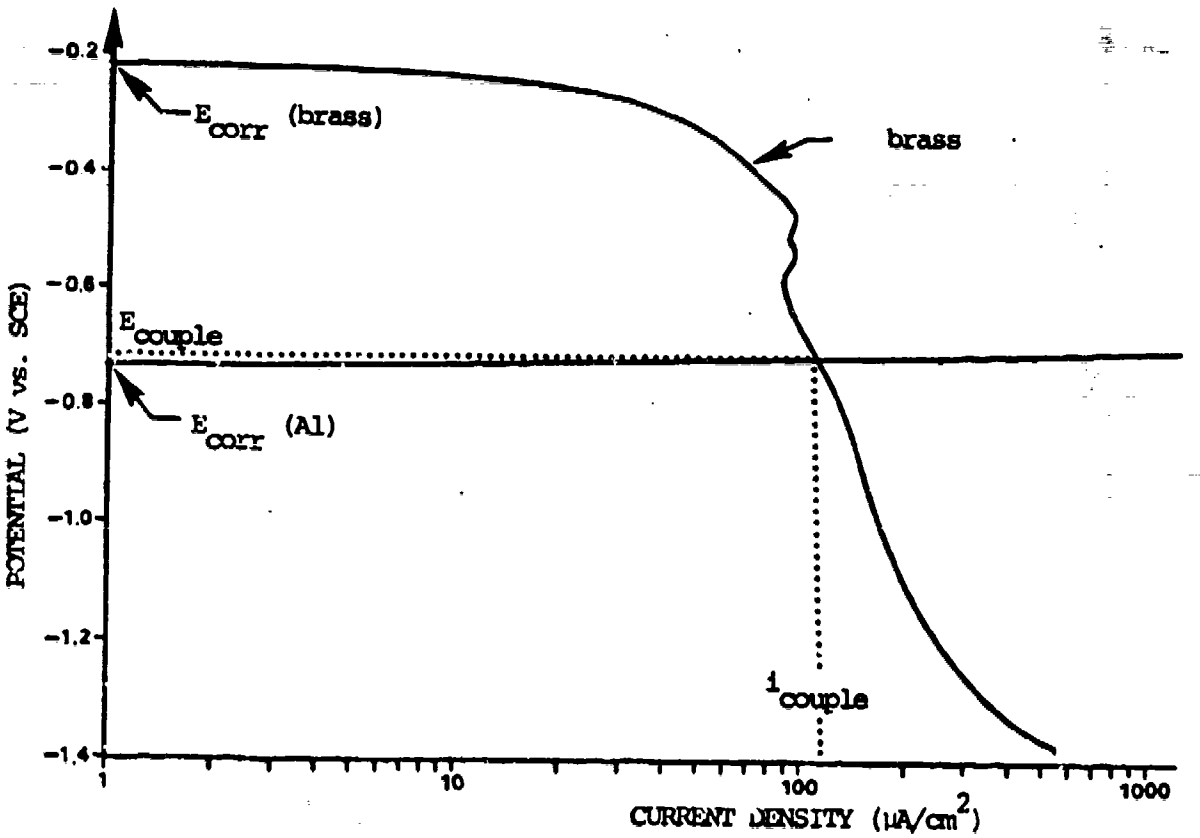

Figure 5: Potentiodynamic polarization curves for 5086 aluminum and naval brass in aerated synthetic seawater.

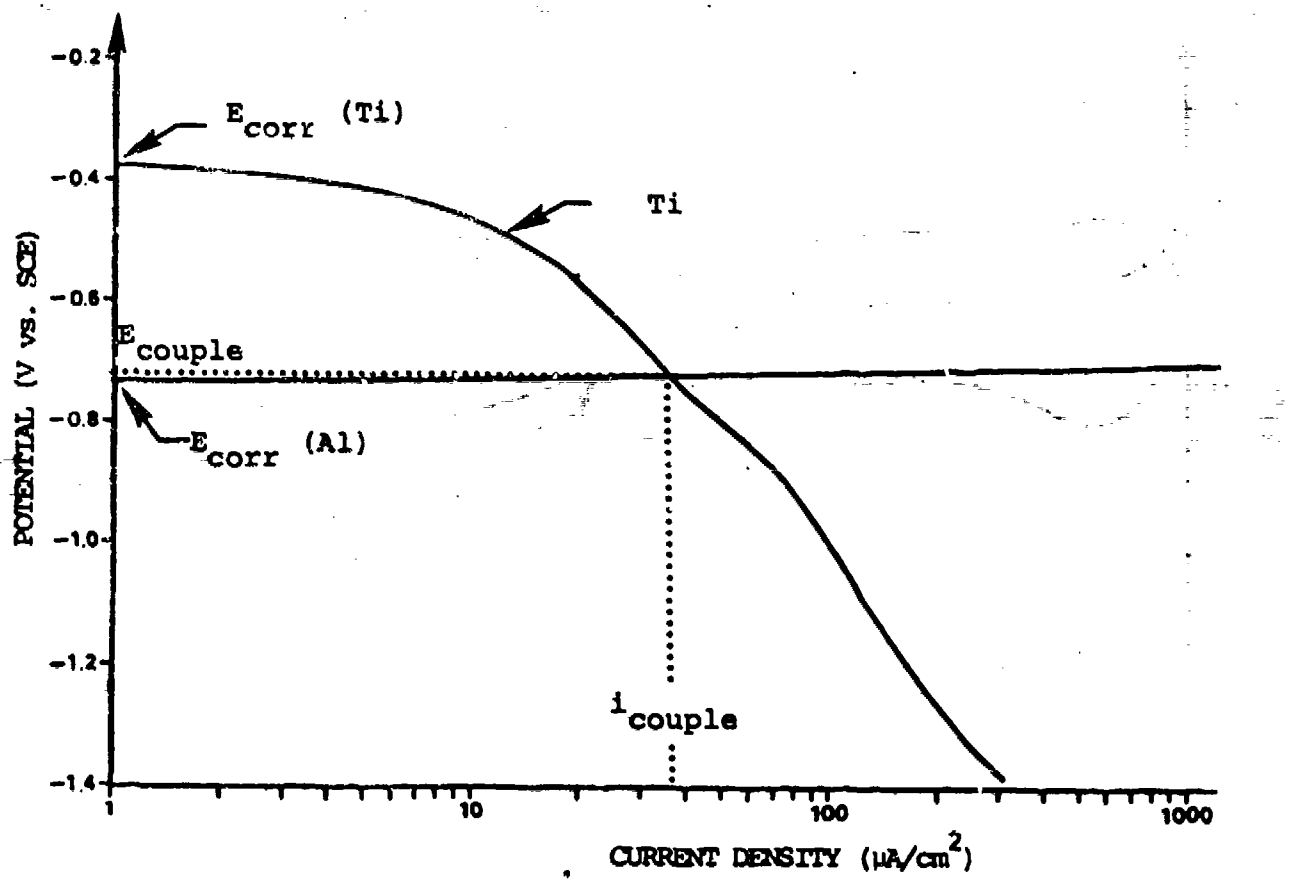

Figure 6: Potentiodynamic polarization curves for 5086 aluminum and Ti-150A titanium in aerated synthetic seawater.

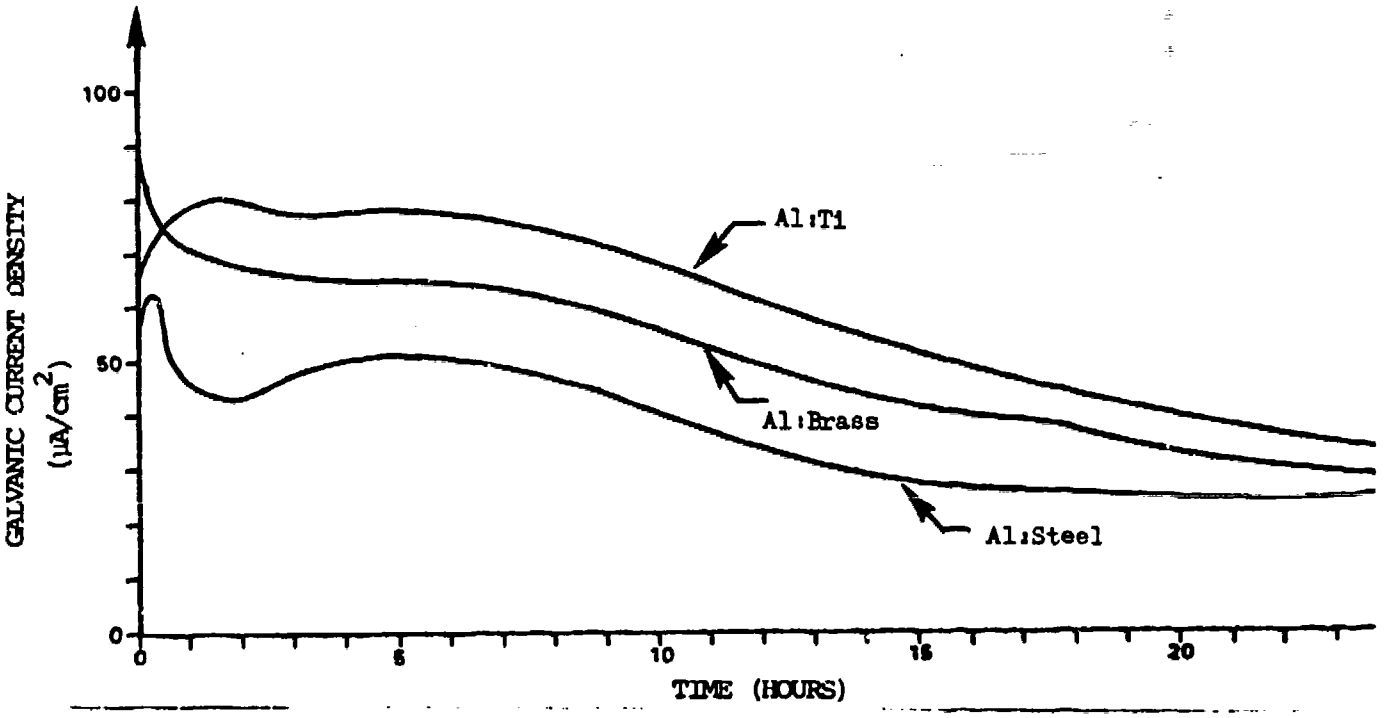

Figure 7: Variation of galvanic current density over a 24 hour period for 5086-H32 aluminum couples with 1040 steel, naval brass, and Ti-150A.

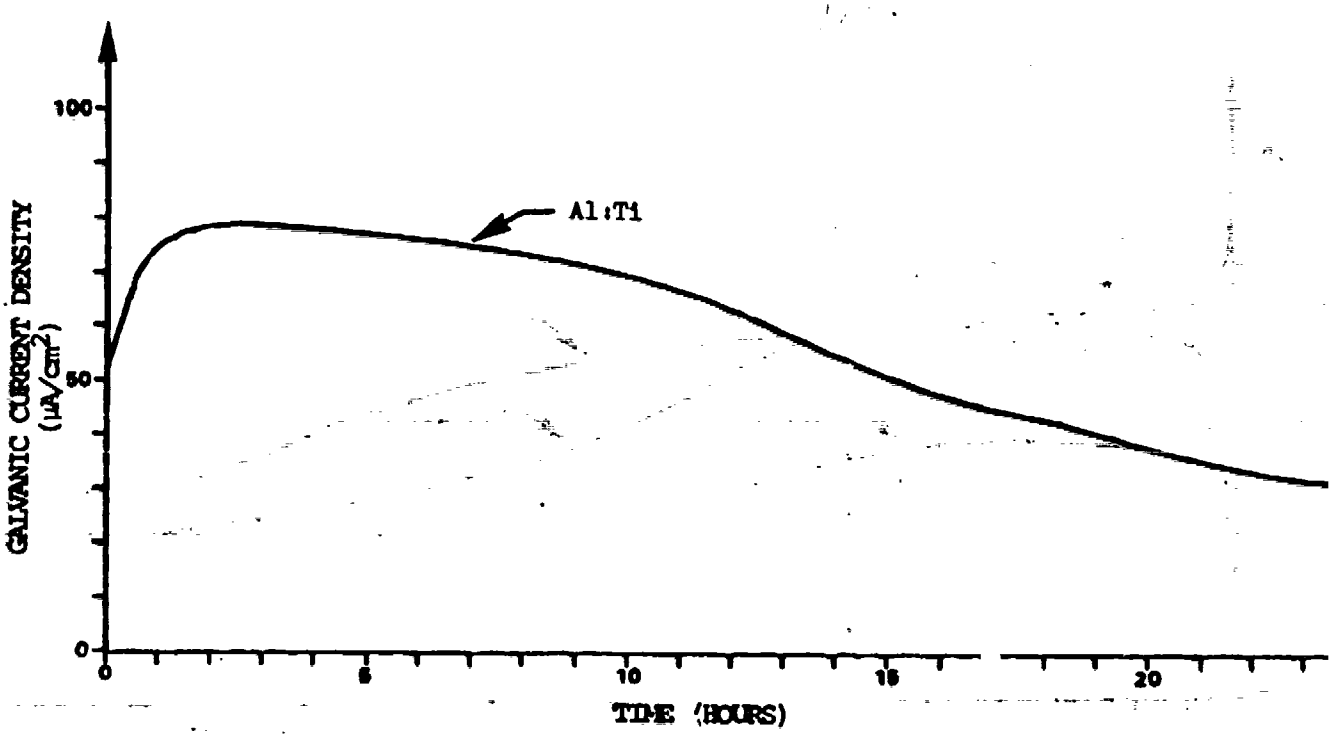

Figure 8: Variation of galvanic current density over a 24 hour period for 5086-H116 aluminum couple with Ti-150A.

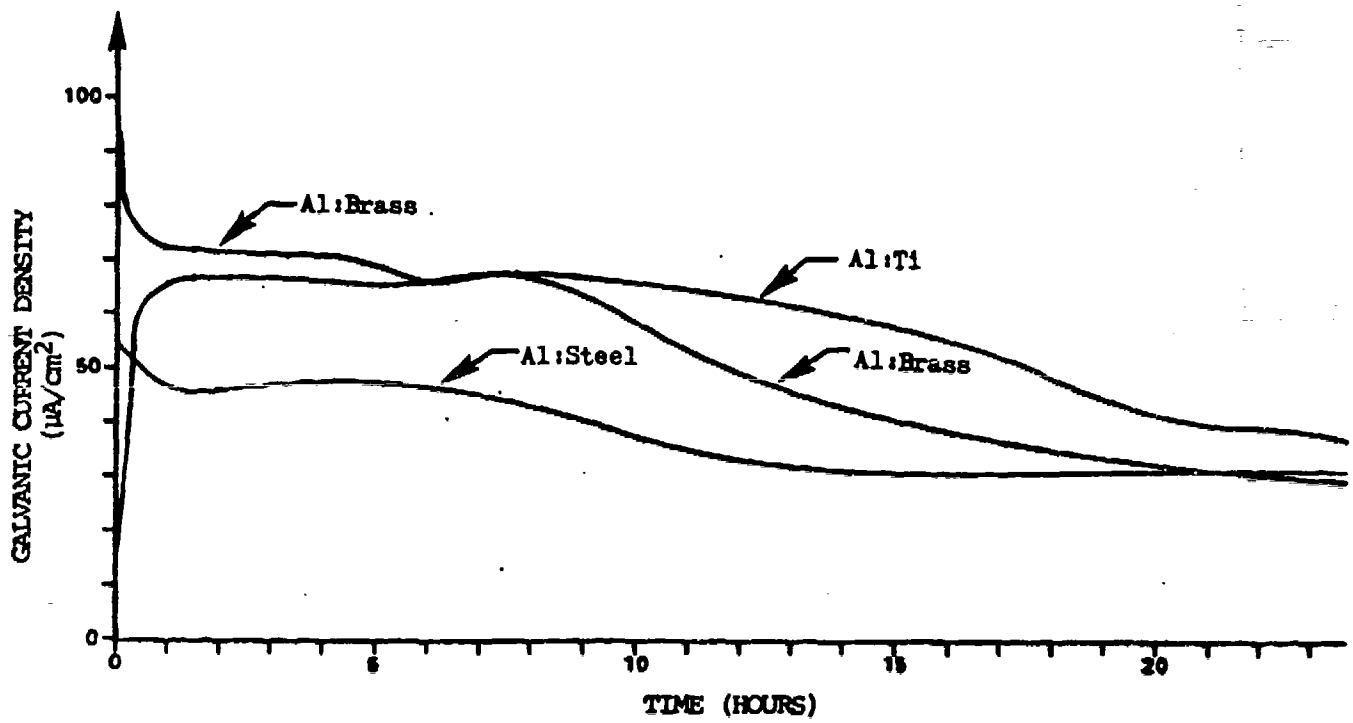

Figure 9: Variation of galvanic current density over a 24 hour period for 5086-H117 couples with 1040 steel, naval brass, and Ti-150A.

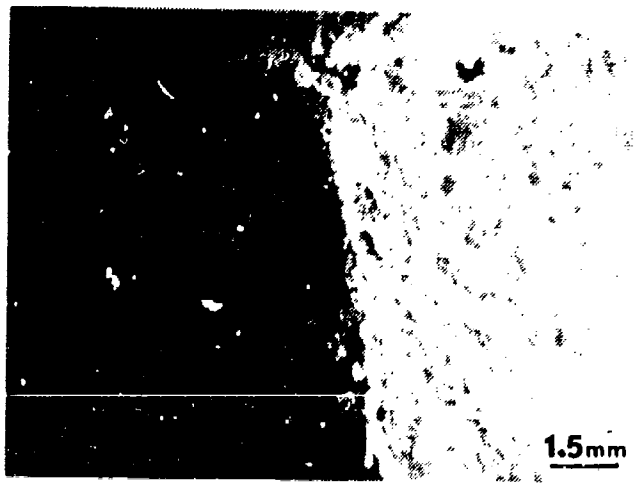

Figure 10: Low magnification photograph of steel/5086-H116 proximate couple exposed for two weeks in aerated synthetic seawater, 7X.

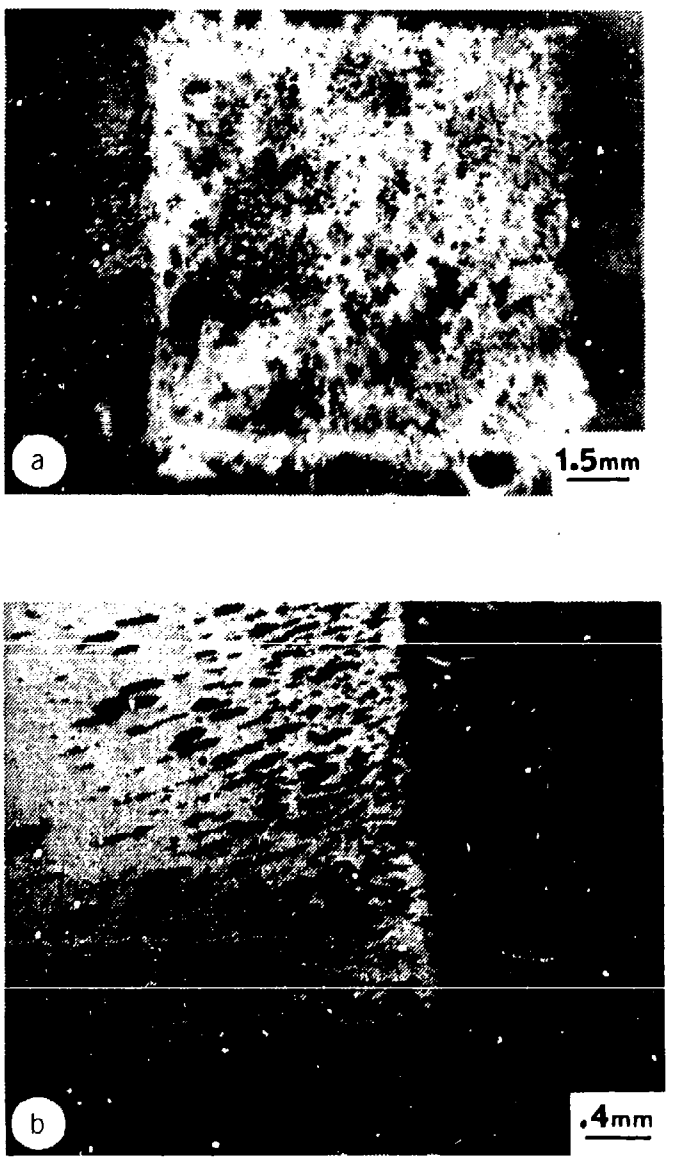

Figure 11: Naval brass/5086-H32 couple exposed two weeks in aerated synthetic seawater (a) 6X (b) 24X. Note streaming of corrosion product from anode to cathode due to gentle circulation pattern in electrolyte.

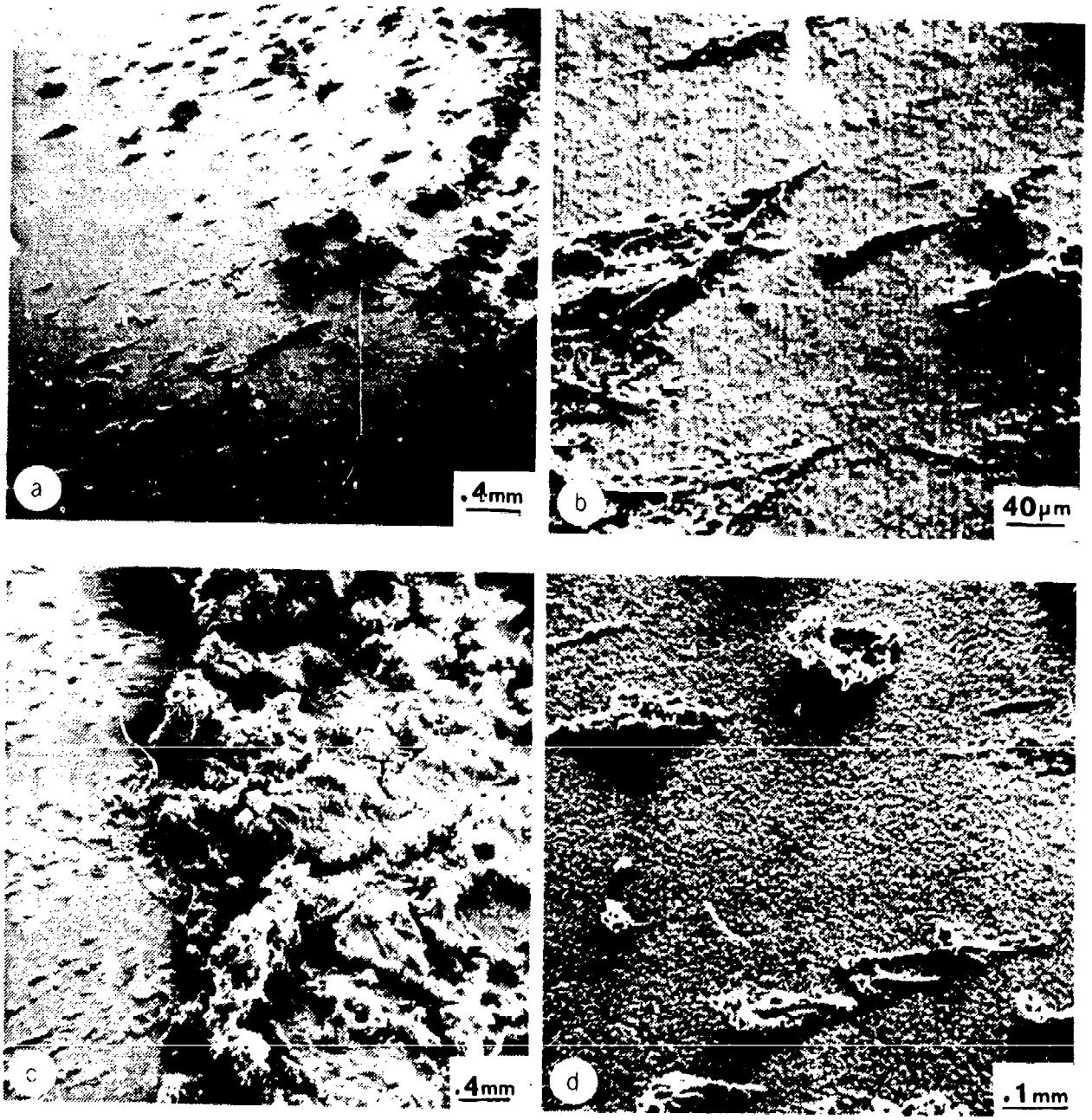

Figure 12: General ridge-like morphology of corrosion product outcroppings found in accumulations on cathodic members of proximate couples in aerated synthetic seawater: (a) on titanium member of Ti/5086-H116 couple exposed for 3 weeks, 24X (b) same, 240X, (c) on titanium member of Ti/5086-H32 couple exposed two weeks, 24X (d) same, 110X (e) on naval brass members of brass/5086-H32 couple exposed 550X three weeks, (f) on titanium member of Titanium/5086-H116 couple exposed two weeks, 105X (g) on 1040 steel member of steel/5086-H32 couple exposed one week, 540X.

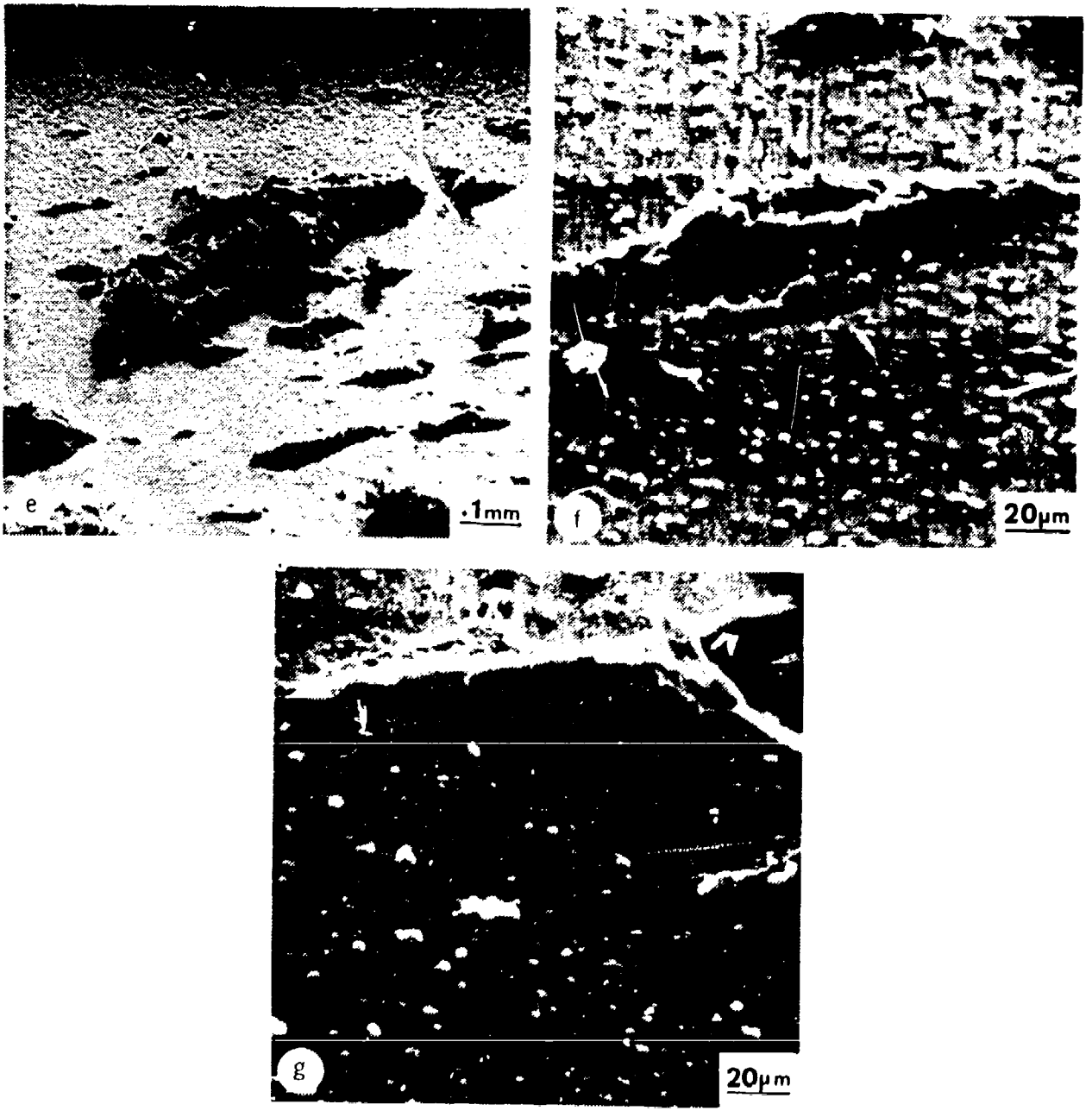

Figure 12: General ridge-like morphology of corrosion product outcroppings found in accumulations on cathodic members of proximate couples in aerated synthetic seawater: (a) on titanium member of Ti/5086-H116 couple exposed for 3 weeks, 24X (b) same, 240X, (c) on titanium member of Ti/5086-H32 couple exposed two weeks, 24X (d) same, 110X (e) on naval brass members of brass/5086-H32 couple exposed 550X three weeks, (f) on titanium member of Titanium/5086-H116 couple exposed two weeks, 105X (g) on 1040 steel member of steel/5086-H32 couple exposed one week, 540X.

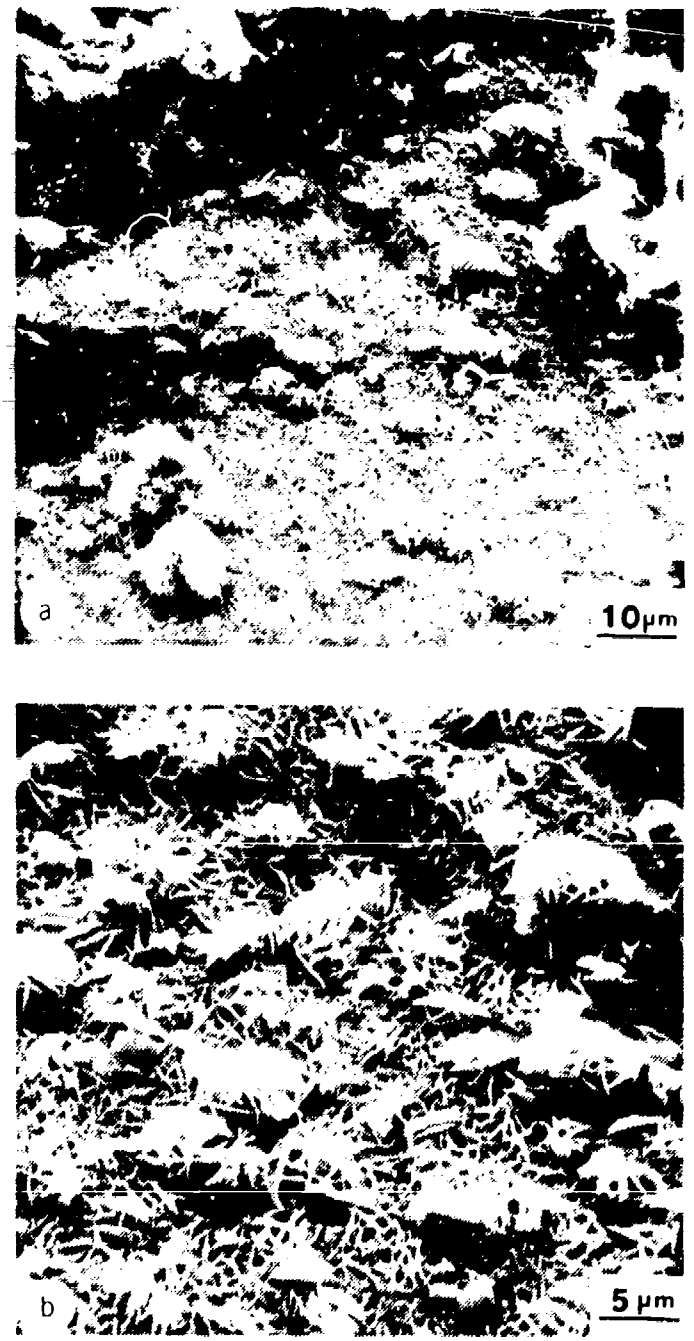

Figure 13: Details of the structural morphology of the continuous base layer covering the cathodic members of proximate couples, in this case on the 1040 steel member of a steel/5086-H32 couple exposed for three weeks in aerated synthetic seawater: (a) 1150X (b) 2300X. The base layer is observed to be made up of a regularly arranged array of very fine crystallites.

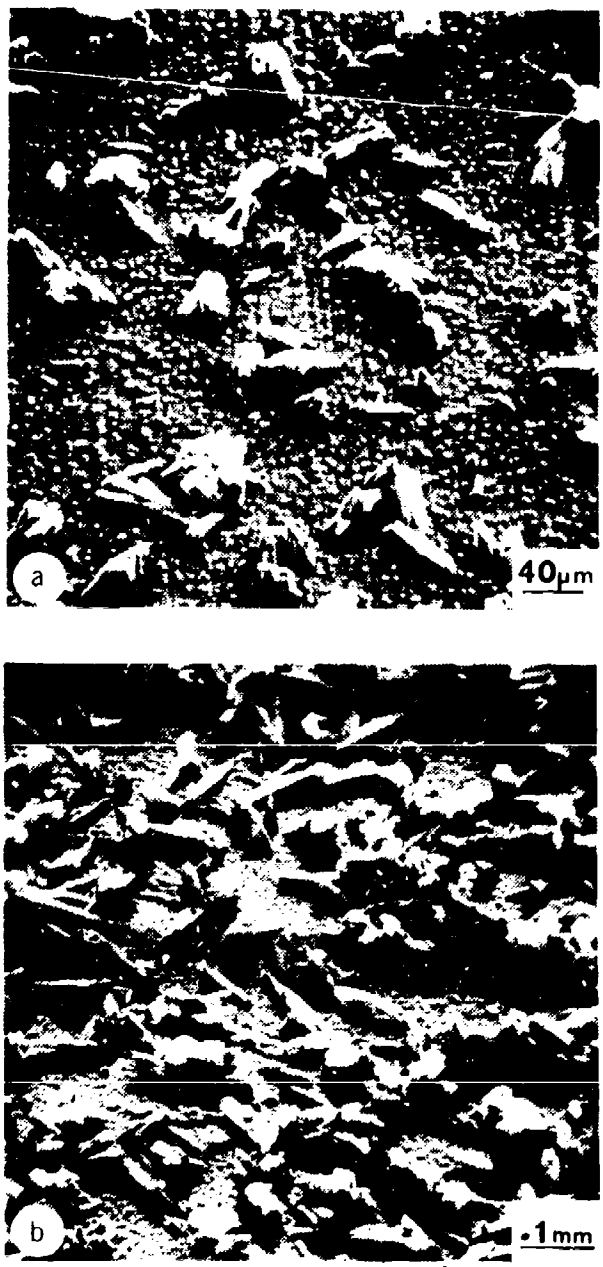

Figure 14: Precipitate formations occasionally found on cathodic members of proximate couples, shown here for brass/5086-H32 couples in aerated synthetic seawater: (a) exposed two weeks, 230X, (b) exposed eight weeks, 110X, (c) same, 550X, (d) calcium x-ray distribution image of same area.

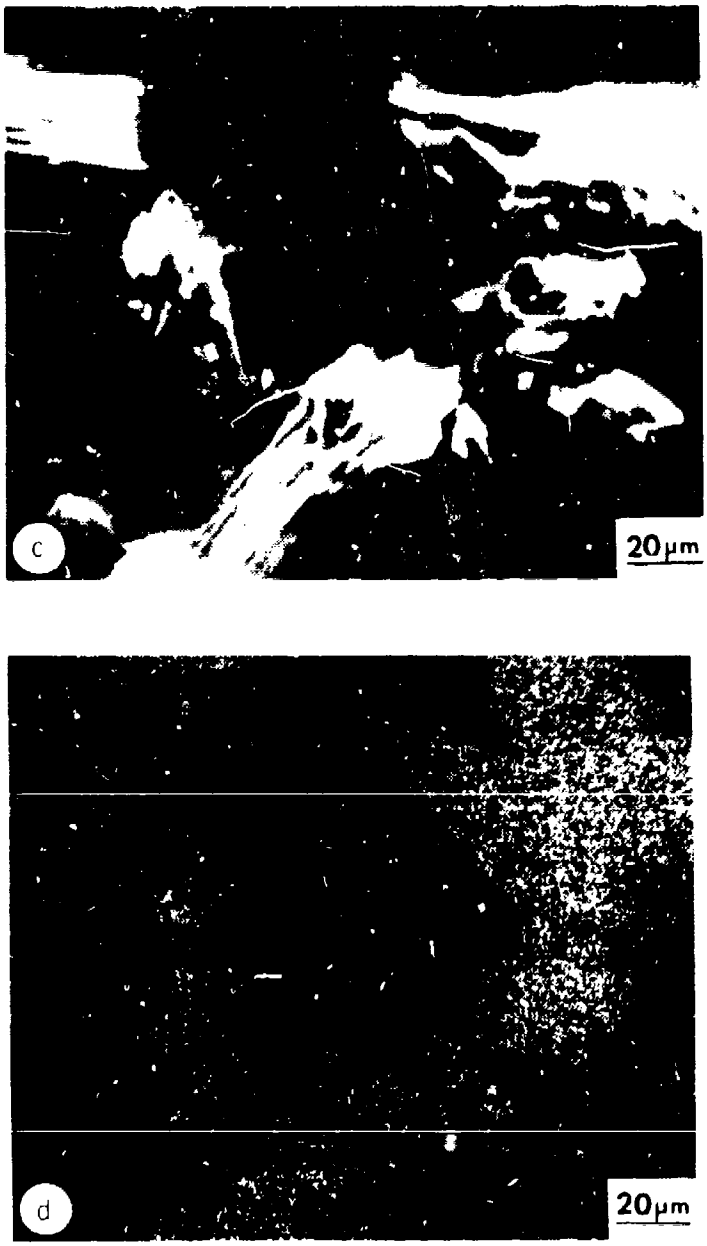

Figure 14: Precipitate formations occasionally found on cathodic members of proximate couples, shown here for brass/5086-H32 couples in aerated synthetic seawater: (a) exposed two weeks, 230X, (b) exposed eight weeks, 110X, (c) same, 550X, (d) calcium x-ray distribution image of same area.

Figure 15: Low-magnification photograph of naval brass/5086-H32 proximate couple exposed for one week in aerated synthetic seawater, 7X.

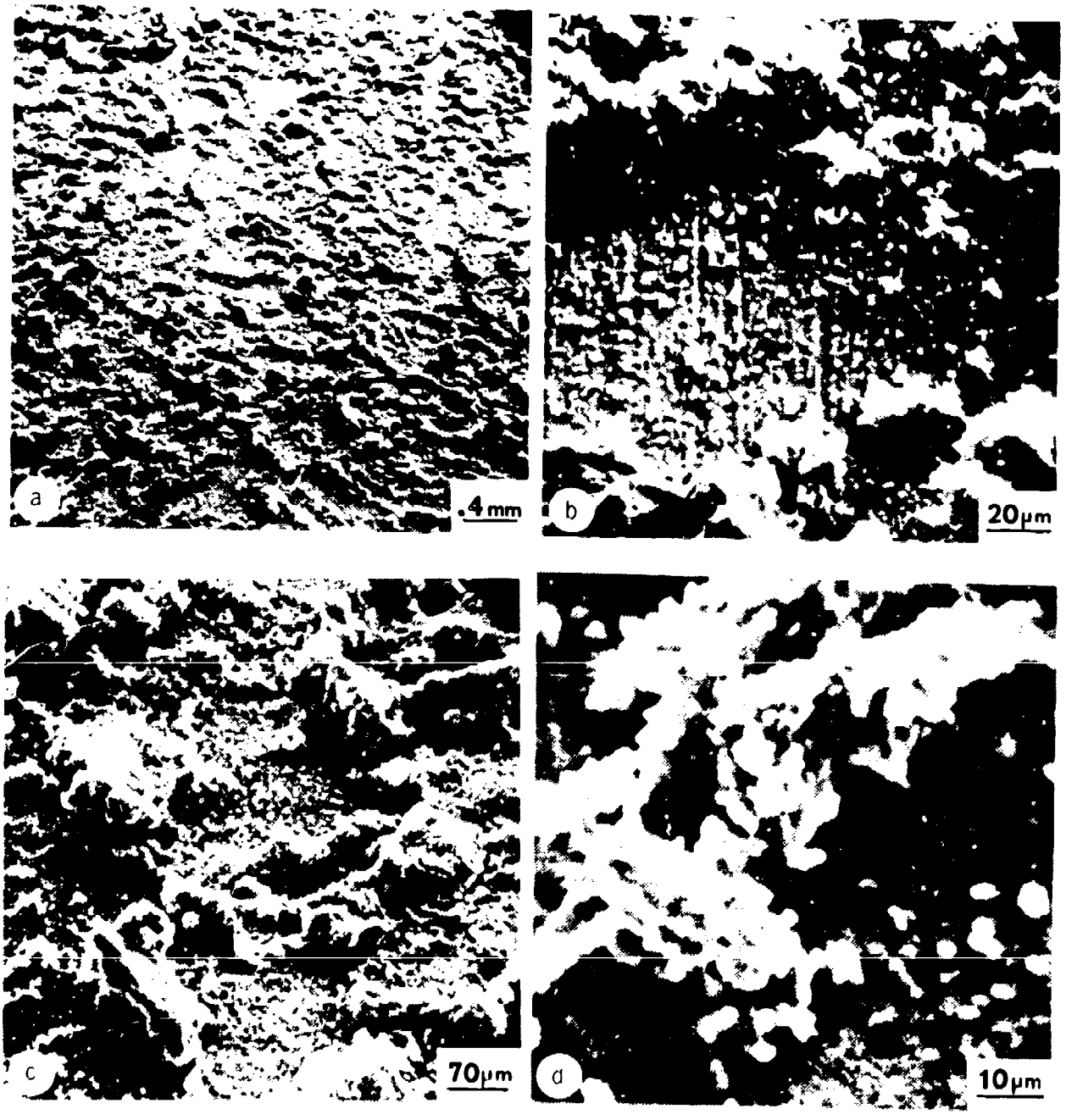

Figure 16: Typical corrosion product accumulations on 5086-H116 aluminum in proximate couples exposed in aerated synthetic seawater (a) 5086-H116 coupled to Ti-150A, exposed three weeks, 23X, (b) same, 1150X, (c) 5086-H116, coupled to 1040 steel, exposed one week, 150X, (d) same, 1150X, (e) 5086-H116 coupled to Ti-150A, exposed two weeks, 55X.

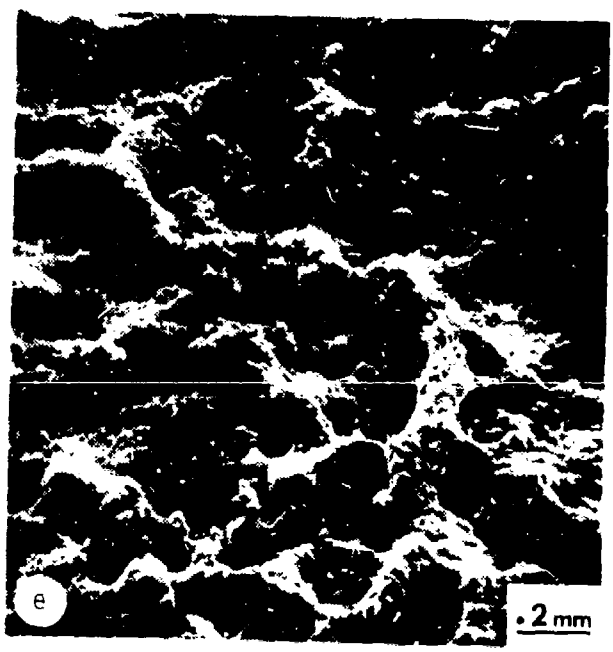

Figure 16: Typical corrosion product accumulations on 5086-H116 aluminum in proximate couples exposed in aerated synthetic seawater (a) 5086-H116 coupled to Ti-150A, exposed three weeks, 23X, (b) same, 1150X, (c) 5086-H116, coupled to 1040 steel, exposed one week, 150X, (d) same, 1150X, (e) 5086-H116 coupled to Ti-150A, exposed two weeks, 55X.

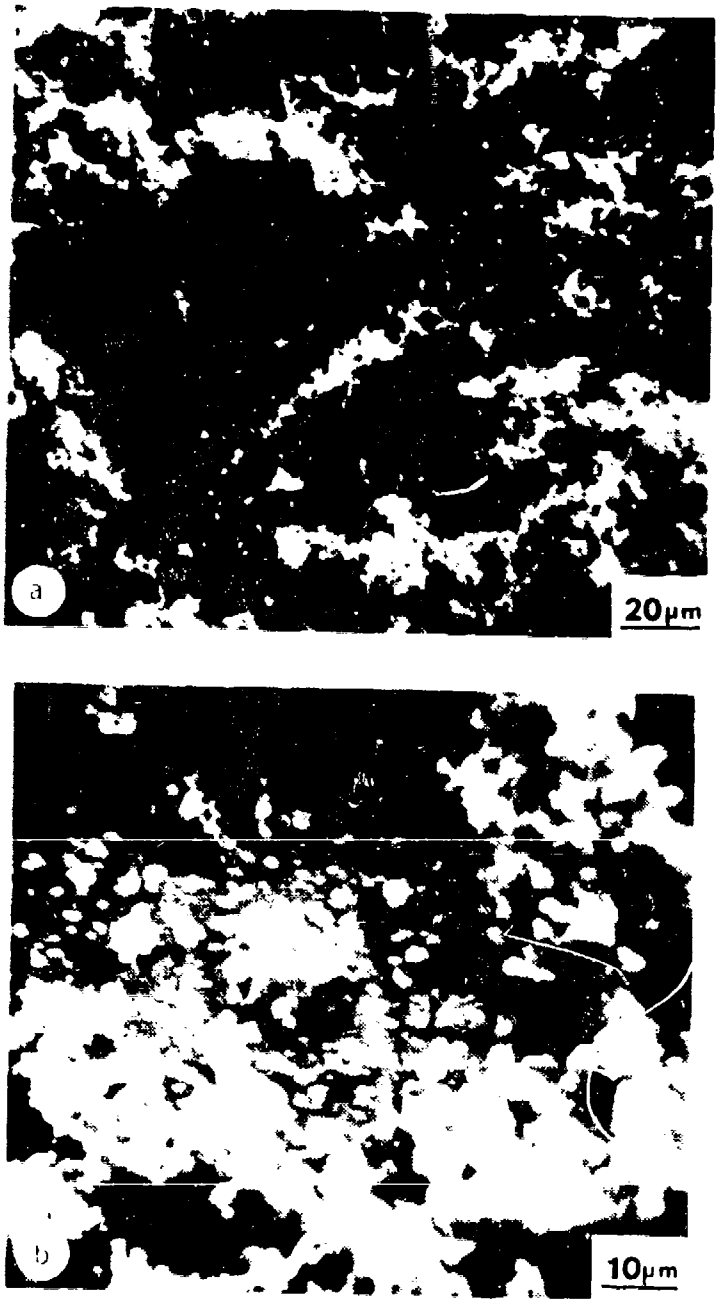

Figure 17: Typical variations in corrosion product morphology found on 5086 aluminum exposed in proximate couples in aerated synthetic seawater:
(a) 570X
(b) 1100X.

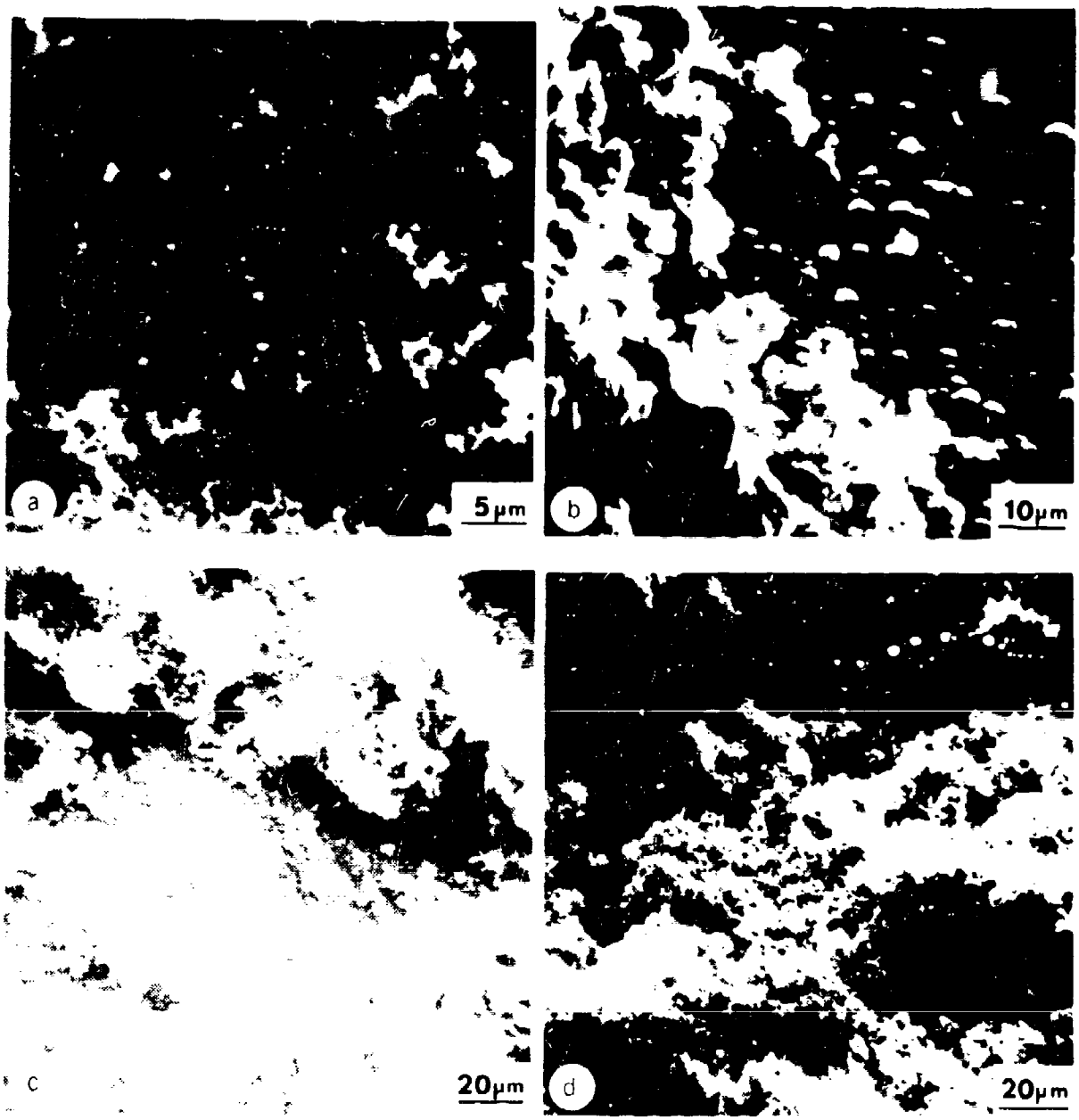

Figure 18: Examples of various corrosion product morphologies observed on 5086 aluminum exposed in proximate couples in aerated synthetic seawater.
(a) 5086-H32, coupled with 1040 steel, exposed one week, 2200X,
(b) 5086-H116, coupled with 1040 steel, exposed three weeks, 1100X,
(c) 5086-H32, coupled with 1040 steel, exposed three weeks, 540X,
(d) 5086-H32, coupled to naval brass, exposed one week, 575X.

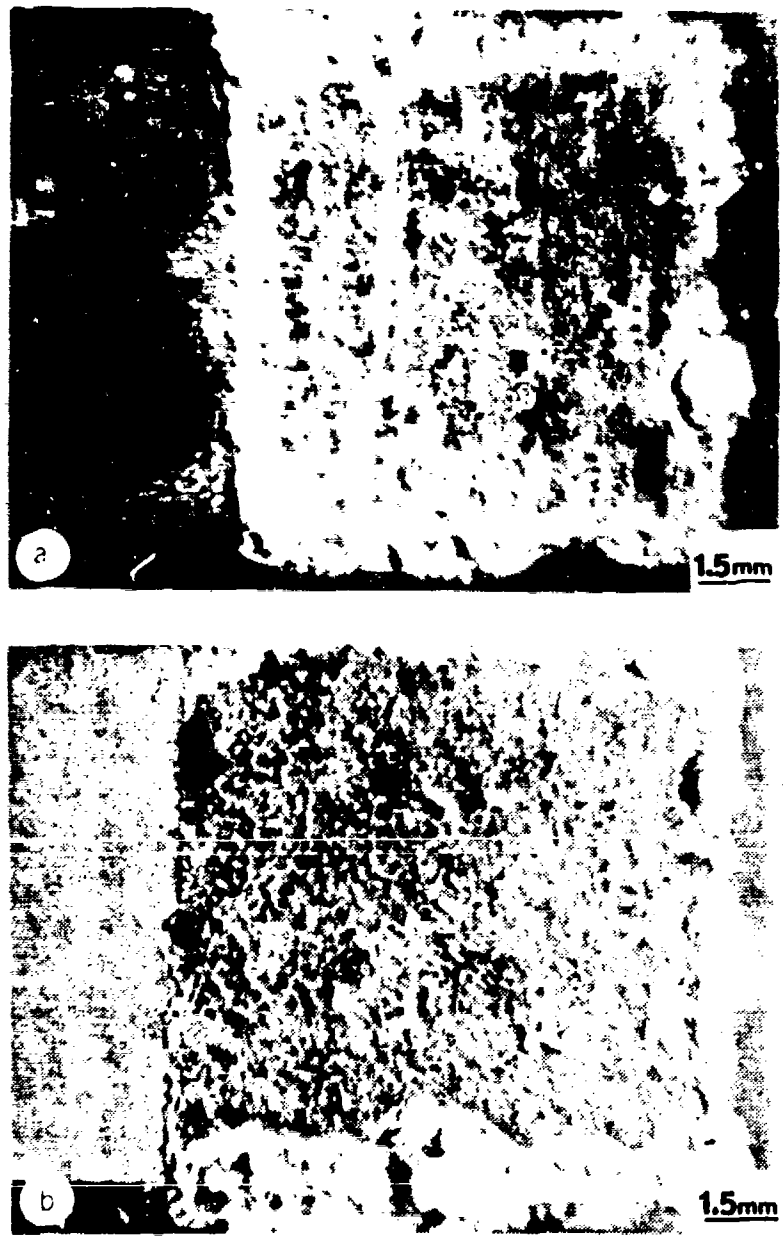

Figure 19: Photographs of (a) 1040 steel/5086-H32 and (b) naval brass/5086-H32 proximate couples after one week exposure in aerated synthetic seawater, to illustrate the discontinuous distribution of concentrated attack along the edges of the aluminum coupons.

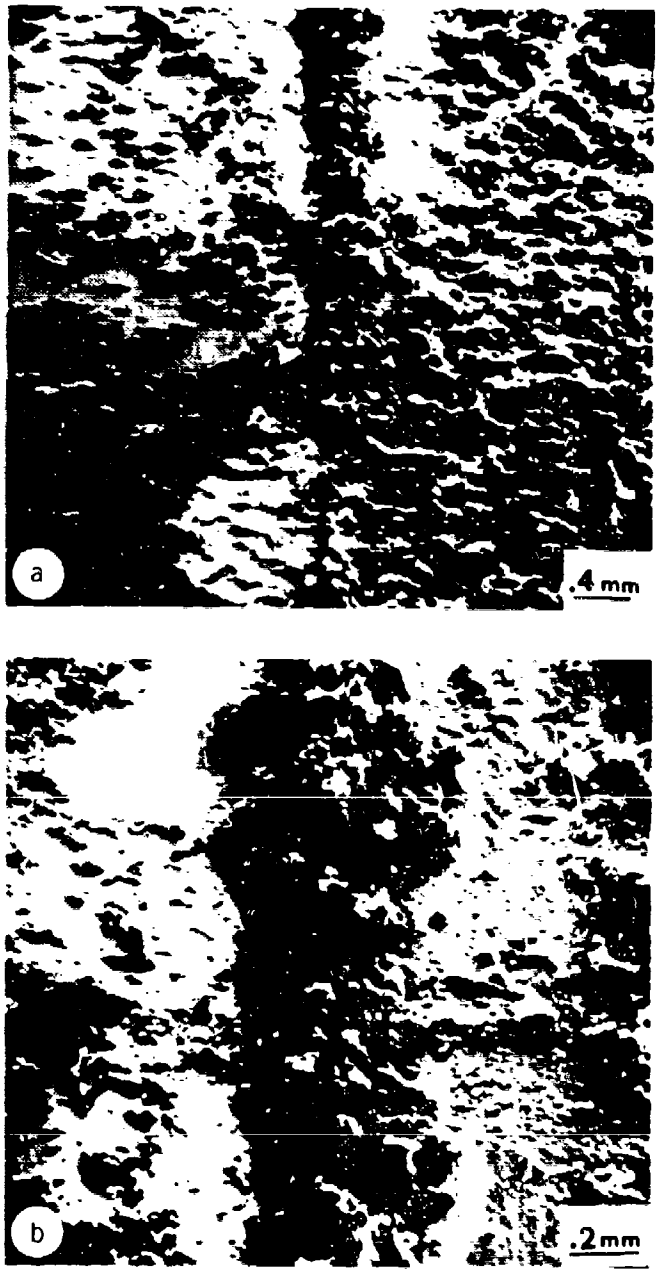

Figure 20: Concentrated corrosion product accumulation at bimetallic interface of Ti-150A/5086-H32 proximate couple exposed 3 weeks in aerated synthetic seawater: (a) 22X, (b) 52X. Note the relatively low accumulation of corrosion products in a "corridor" on the aluminum adjacent to the interface.

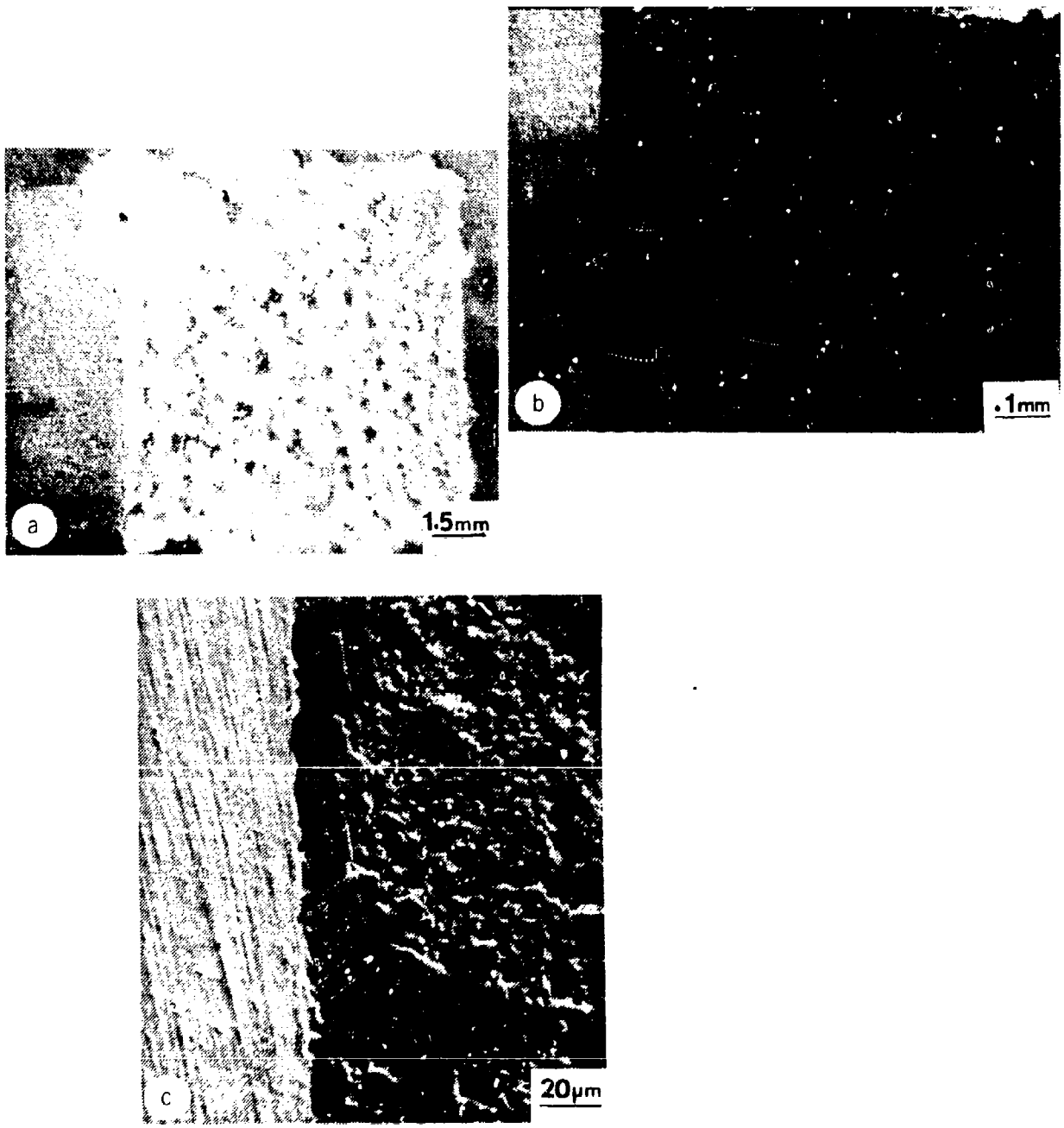

Figure 21: Illustration of correlation of corrosion product distribution and dissolution pattern, for Ti-150A/5086-H32 proximate couple exposed two days in aerated synthetic seawater: (a) low magnification photograph of couple, showing distribution of corrosion products along bimetallic interface; (b) dissolution cavity found in the aluminum after ultrasonic cleaning, located under the heavy corrosion product o tcropping seen in (a) at the top along the interface, 100X; (c) no dissolution cavity is found further down the same interface, 550X.

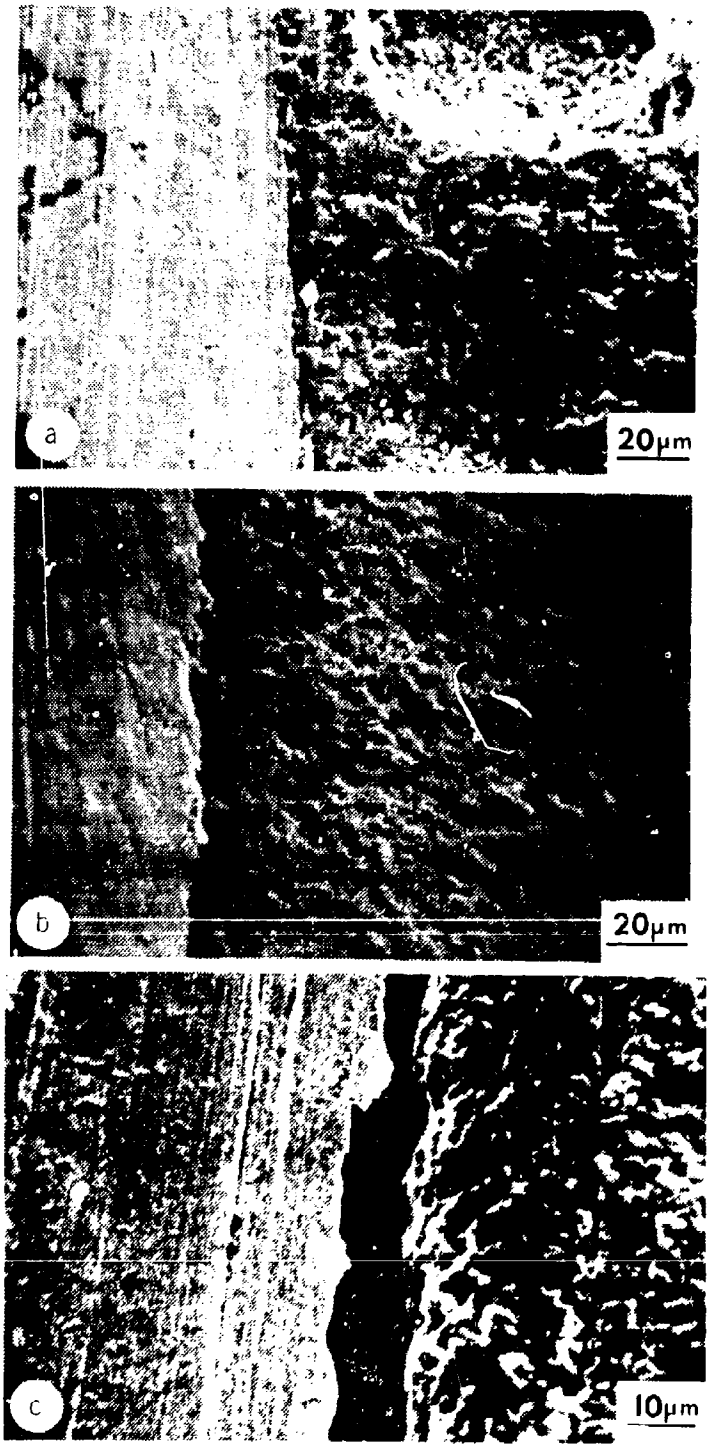

Figure 22: Appearance of bimetallic interfaces of proximate couples after two-day exposures in aerated synthetic seawater, then ultrasonically cleaned of corrosion products: (a) naval brass/5086-H32 couple, 550X; (b) Ti-1.5Al/5Mn - H38 couple, 600X; (c) 1040 steel/5086-H32 couple, 1050X.

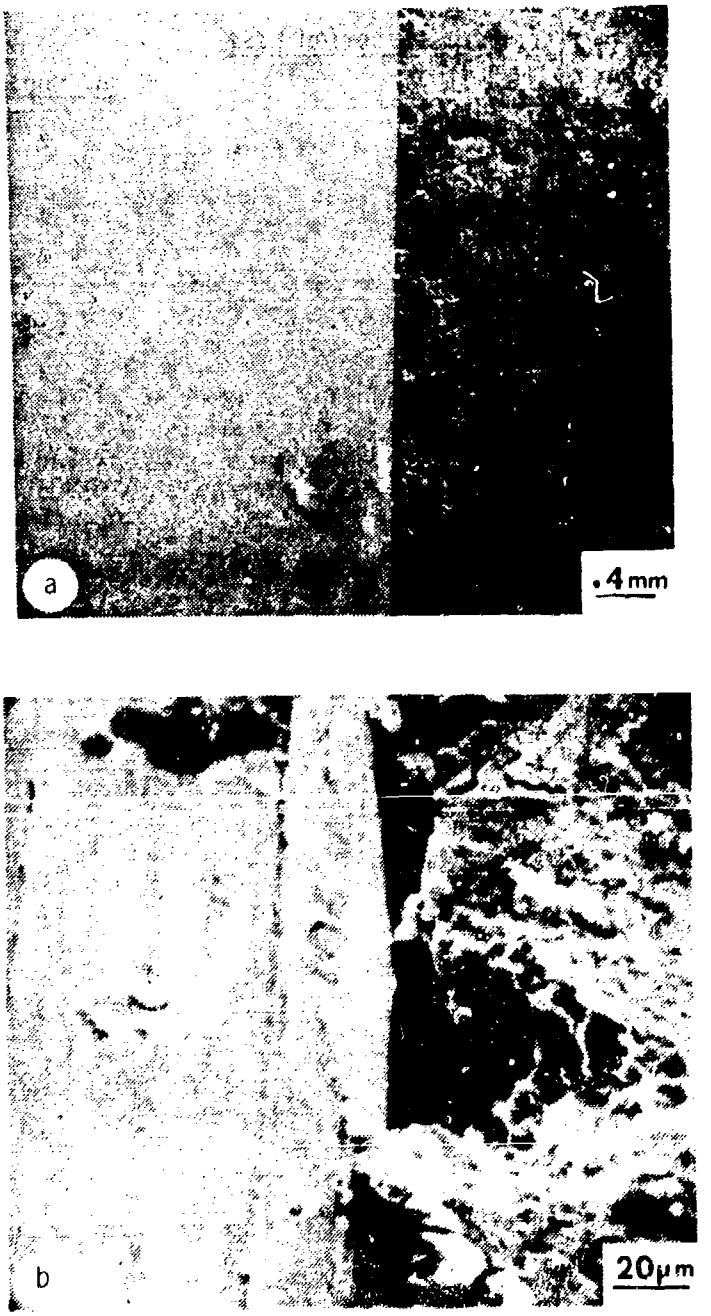

Figure 23: Appearance of bimetallic interfaces of proximate couples after exposure in aerated synthetic seawater, then ultrasonically cleaned of corrosion products: (a) Ti-150A/5086-H32 couple, exposed for 2 weeks, then cleaned, 22X; (b) naval brass/5086-H32 couple, exposed 8 weeks, then cleaned, 550X.

INITIAL DISTRIBUTION LIST

		No. Copies
1.	Defense Documentation Center Cameron Station Alexandria, Virginia 22314	2
2.	Library, Code 0142 Naval Postgraduate School Monterey, California 93940	2
3.	Department Chairman, Code 69 Department of Mechanical Engineering Naval Postgraduate School Monterey, California 93940	2
4.	Naval Research Laboratory Washington, D. C. 20390 Code 2627	1
5.	Naval Air Propulsion Test Center Trenton, NJ 08628 Attn: Library	1
6.	Office of Naval Research Department of the Navy (Attn:Code 471) 800 N. Quincy Street Arlington, VA 22217	1
7.	Naval Air Development Center Code 302 Warminster, PA 18974 Attn: Mr. F. S. Williams	1
8.	Naval Construction Battalion Civil Engineering Laboratory Port Hueneme, CA 93043 Attn: Materials Division	1
9.	Office of Naval Research 800 N. Quincy Street Arlington, VA 22217 Attn: Code 102	1
10.	Naval Electronics Lab. Center San Diego, CA 92152 Attn: Electron Materials Sciences Division	1
11.	Naval Missile Center Materials Consultant Code 3312-1 Point Mugu, CA 93041	1

12. Office of Naval Research — 1
800 N. Quincy Street
Arlington, VA 22217
Attn: Code 470

13. Commanding Officer — 1
Naval Surface Weapons Center
White Oak Laboratory
Silver Spring, MD 20910

14. David W. Taylor — 1
Naval Ship R & D Center
Materials Department
Annapolis, MD 21402

15. Commanding Officer — 1
Office of Naval Research
Branch Office
495 Summer Street
Boston, MA 02210

16. Naval Undersea Center — 1
San Diego, CA 92132
Attn: Library

17. Naval Underwater System Center — 1
Newport, RI 02840
Attn: Library

18. Commanding Officer — 1
Office of Naval Research
Branch Office
536 S. Clark Street
Chicago, IL 60605

19. Naval Weapons Center — 1
China Lake, CA 93555
Attn: Library

20. Naval Air Systems Command — 1
Washington, D. C. 20360
Attn: Code 52031

21. Office of Naval Research — 1
San Francisco Area Office
760 Market Street, Rm 447
San Francisco, CA 94102

22. Naval Air Systems Command — 1
Washington, D. C.
Attn: Code 52032

23. Naval Air Systems Command — 1
Washington, D. C. 20360
Attn: Code 320

24. Naval Research Lab. 1
Washington, DC 20390
Attn: Code 6000

25. Naval Sea System Command 1
Washington, DC 20362
Attn: Code 035

26. NASA Headquarters 1
Washington, D. C.
Attn: Code RRM

27. Naval Research Lab. 1
Washington, DC 20390
Attn: Code 6100

28. Naval Facilities 1
Engineering Command
Alexandria, VA 22331
Attn: Code 03

29. NASA 1
Lewis Research Center
20111 Brookpark Road
Cleveland, Ohio 44135
Attn: Library

30. Naval Research Lab. 1
Washington, D.C. 20390
Attn: Code 6300

31. Scientific Advisor 1
Commandant of the Marine Corps
Washington, D. C. 20380
Code AX

32. National Bureau of Standards 1
Washington, DC 20234
Attn: Metallurgy Division
Inorganic Mat. Div.

33. Dr. Wm. R. Prindle 1
National Academy of Sciences
National Research Council
2101 Constitution Ave.
Washington, DC20418

34. Dr. R. P. Wei, Lehigh Univ. 1
Inst. for Fracture &
Solid Mechanics
Bethlehem, PA 18015

35. Prof. H. G. F. Wilsdorf 1
Univ. of Virginia
Dept. of Mat. Science
Charlottesville, VA 22903

36. Defense Metals and Ceramics Info Center
Battelle Mem. Institute
505 King Ave.
Columbus, Ohio 43201 — 1

37. Naval Ship Engr. Center
CTR BG #2 Code 6101
3700 E-W Highway
Prince George Plaza
Hyattsville, MD 20782 — 1

38. Director, Ordnance Research Lab.
P.O. Box 30
State College, PA 16801 — 1

39. Army Research Office
Box CM, Duke Station
Durham, NC 27706
Attn: Metallurgy & Cer. Div. — 1

40. Army Materials and Mechanics Research Center
Watertown, MA 02172
Attn: (AMXMR-P) — 1

41. Dir. Applied Physics Lab.
University of Washington
1013 NE 40th Street
Seattle, WA 98105 — 1

42. Metals and Ceramics Div.
Oak Ridge Nat'l Lab.
P.O. Box X
Oak Ridge, TN 37380 — 1

43. AF/Ofc. of Scientific Research
Bldg. 410 Bolling AF Base
Washington, D. C. 20332
Attn: Chem. Sci. Directorate
Electronics & S. S. Sci. Director — 1

44. Los Alamos Scientific Lab
P.O. Box 1663
Los Alamos, NM 87544
Attn: Report Librarian — 1

45. AF Materials Lab. (LA)
Wright-Patterson AFBase
Dayton, Ohio 45433 — 1

46. Argonne National Lab.
Metallurgy Division
P.O. Box 229
Lemont, IL 60439 — 1

47. Dr. J. A. S. Green — 1
Martin Marietta Corp.
1450 S. Rolling Road
Baltimore, MD 21227

48. Dr. T. R. Beck — 1
Electrochemical Tech. Corp.
10035 31st Ave. NE
Seattle, WA 98125

49. Prof. R. H. Heidersbach — 1
University of Rhode Island
Department of Ocean Engr.
Kingston, RI 02881

50. Professor I. M. Bernstein — 1
Carnegie-Mellon Univ.
Schenley Park
Pittsburgh, PA 15213

51. Professor H. K. Birnbaum — 1
Univ. of Illinois
Dept. of Metallurgy
Urbana, IL 61801

52. Prof. J. P. Hirth — 1
Ohio State University
Metallurgical Engineering
Columbus, OH 43210

53. Prof. H. Herman — 1
State Univ. of New York
Materials Science Div.
Stony Brook, NY 11794

54. Dr. Otto Buck — 1
Rockwell International
1049 Camino Dos Rios
P.O. Box 1085
Thousand Oaks, CA 91360

55. Dr. D. W. Hoeppner — 1
University of Missouri
College of Engineering
Columbia, MO 65201

56. Prof. H. W. Pickering — 1
Pennsylvania State Univ.
Dept. of Mat. Sciences
University Park, PA 16802

57. Dr. David L. Davidson — 1
Southwest Research Inst.
8500 Culebra Road
P.O. Drawer 28510
San Antonio, TX 78284

1310 Beulah Road
Pittsburgh, PA 15235

59. Dr. F. Mansfeld — 1
Rockwell
1049 Camino Dos Rios
P.O. Box 1085
Thousand Oaks, CA 91360

60. Dr. D. J. Duquette — 1
Dept. of Metallurgical Engr.
Rensselaer Polytechnic Inst.
Troy, NY 12181

61. Prof. R. T. Foley — 1
The American University
Dept. of Chemistry
Washington, DC 20016

62. Prof. A. E. Miller — 1
University of Notre Dame
College of Engineering
Notre Dame, IN 46556

63. Mr. G. A. Gehring — 1
Ocean City Research Corp.
Tennessee Ave. & Beach Thorofare
Ocean City, NJ 08226

64. Prof. R. W. Staehle — 1
Ohio State University
Dept. of Metallurgical Engr.
Columbus, OH 43210

65. Dr. Barry C. Syrett — 1
Stanford Research Institute
333 Ravenswood Avenue
Menlo Park, CA 94025

66. Brookhaven Nat'l Laboratory — 1
Technical Info. Div.
Upton, LI
New York 11973
Attn: Research Library

67. Library — 1
Building 50 Rm 134
Lawrence Radiation Laboratory
Berkeley, CA 94550

68. Prof. Jeff Perkins — 30
Naval Postgraduate School
Code (69Ps)
Monterey, CA 93940

69. Office of Research Administration
Code 012A
Naval Postgraduate School
Monterey, California 93940